



NIH Public Access

Author Manuscript

Image Vis Comput. Author manuscript; available in PMC 2009 November 3.

Published in final edited form as:

Image Vis Comput. 2001 January 1; 19(1-2): 3–24. doi:10.1016/S0262-8856(00)00055-X.

The role of image registration in brain mapping

A.W. Toga^{*} and P.M. Thompson

Laboratory of Neuro Imaging, Department of Neurology, Division of Brain Mapping, UCLA School of Medicine, Los Angeles, CA 90095-1769, USA

Abstract

Image registration is a key step in a great variety of biomedical imaging applications. It provides the ability to geometrically align one dataset with another, and is a prerequisite for all imaging applications that compare datasets across subjects, imaging modalities, or across time. Registration algorithms also enable the pooling and comparison of experimental findings across laboratories, the construction of population-based brain atlases, and the creation of systems to detect group patterns in structural and functional imaging data. We review the major types of registration approaches used in brain imaging today. We focus on their conceptual basis, the underlying mathematics, and their strengths and weaknesses in different contexts. We describe the major goals of registration, including data fusion, quantification of change, automated image segmentation and labeling, shape measurement, and pathology detection. We indicate that registration algorithms have great potential when used in conjunction with a digital brain atlas, which acts as a reference system in which brain images can be compared for statistical analysis. The resulting armory of registration approaches is fundamental to medical image analysis, and in a brain mapping context provides a means to elucidate clinical, demographic, or functional trends in the anatomy or physiology of the brain.

Keywords

Brain mapping; Image registration; Brain atlas

1. Introduction

Image registration is a prerequisite to numerous imaging applications in the neurosciences. Registration is required for three-dimensional (3D) reconstruction, multimodality image mappings, atlas construction and arithmetic operations such as image averaging, subtraction and correlation. Physical sectioning procedures, unlike various tomographic imaging techniques, also require additional superpositioning schemes to register serial sections. Since the mid 1980s investigators have used several approaches, with varying degrees of manual interaction, to perform image registration. These approaches use either information obtained about the shape and topology of objects in the image, or the presumed consistency in the intensity information from one slice to its immediate neighbor or from one brain or image set to another.

Registration algorithms have a powerful range of applications when used in conjunction with a brain atlas. Digital atlases of the brain, which represent anatomy in a 3D coordinate system, are fundamental in brain mapping. Atlases define the brain's spatial characteristics: where is a given structure; relative to what other features; what are its shape and characteristics and how

do we refer to it? Where is this region of functional activation? How different is this brain compared with a normal database? An atlas allows us to answer these and related questions quantitatively.

2. Brain atlases

Brain atlases are built from one or more representations of brain [1]. They describe one or more aspects of brain structure and/or function and their relationships after applying appropriate registration and warping strategies [2], indexing schemes and nomenclature systems. Atlases made from multiple modalities and individuals provide the capability to describe image data with statistical and visual power.

Atlases have enabled a tremendous increase in the number of investigations focusing on the structural and functional organization of the brain. In humans and other species, the brain's complexity and variability across subjects is so great that reliance on atlases is essential to manipulate, analyze and interpret brain data effectively.

Central to these tasks is registration. Design of appropriate reference systems for brain data presents considerable challenges, since these systems must capture how brain structure and function vary in large populations, across age and gender, in different disease states, across imaging modalities, and even across species.

There are many examples of brain atlases. Initially intended to catalog morphological descriptions, today there is considerable diversity in composition and intent. There are atlases of brain structure based upon 3D tomographic images [3,4], anatomic specimens [5-9,136] and a variety of histologic preparations that reveal regional cytoarchitecture [10]. There are atlases that include regional molecular content such as myelination patterns [11,12], receptor binding sites [13], protein densities and mRNA distributions. Other brain atlases describe function, quantified by positron emission tomography (PET; [14]), functional MRI [15] or electrophysiology [16,17]. Others represent neuronal connectivity and circuitry [18] based on compilations of empirical evidence [10,19,20].

While the differences among these examples help provide a comprehensive view of brain structure and function collectively, none is inherently compatible with any other. Without appropriate registration and warping strategies, these brain maps will remain as individual and independent efforts, and the correlative potential of the many diverse mapping approaches will not be achieved.

Since there is neither a single representative brain nor a simple method to construct an average anatomy or to represent the complex variations around it, the construction of brain atlases to represent large human populations has become a major research focus [21]. Population-based atlases can be used to guide knowledge-based image analysis algorithms, and can even support pathology detection in individual subjects or groups. Single modality atlases may also be insufficient, because of the need to establish the relationship between different measurements of anatomy and physiology. In response to these challenges, multi-modality atlases combine detailed structural maps from multiple imaging sensors in the same 3D coordinate space. Fig. 1 shows a multi-modality atlas of the brain in Alzheimer's disease, which uses elastic warping to register post mortem biochemical maps with in vivo structural and metabolic data from many subjects [22,23,111]. Anatomic labels can also be used to identify the source of functional activation sites, for example, helping in the analysis of metabolic or functional studies based on PET or functional MRI [24-28]. Multi-modal atlases provide the best of all worlds, offering a realistically complex representation of brain morphology and function in its full spatial and multi-dimensional complexity.

Due to individual variations in anatomy among normal subjects, early registration approaches used proportional scaling systems to reference a given brain to an atlas brain [7]. More sophisticated elastic or fluid transformations, involving local matching, are rapidly becoming common-place [2]. These approaches locally deform a digital atlas to reflect the anatomy of new subjects, or deform an individual's anatomy to match an atlas.

3. Coordinate systems

The coordinate system used to equate brain topology with an index must include carefully selected features common to all brains. Further, these features must be readily identifiable and sufficiently distributed anatomically to avoid bias. Once defined, rigorous systems for matching, or spatially normalizing a brain to this coordinate system must be developed. This allows individual data to be transformed to match the space occupied by the atlas. In the Talairach stereotaxic system[5,7], piecewise affine transformations are applied to 12 rectangular regions of brain, defined by vectors from the anterior and posterior commissures to the extrema of the cortex. These transformations re-position the anterior commissure of the subject's scan at the origin of the 3D coordinate space, vertically align the interhemispheric plane, and horizontally orient the line connecting the two commissures. Each point in the incoming brain image, after it is registered into the atlas space, is labeled by an (x,y,z) address indexed to the atlas brain. Although originally developed to help interpret brain stem and ventricular studies acquired using pneumoencephalography [5], the Talairach stereotaxic system rapidly became an international standard for reporting functional activation sites in PET studies, allowing researchers to compare and contrast results from different laboratories [29-32].

4. Registration

Registration is not as simple as equating the origin of similar coordinate systems. Rather, registration must accommodate diverse types of image data, each with different spatial scales and extents of coverage. Registration is also needed to compare one brain atlas with another. The success of any brain atlas depends on how well the anatomies of individual subjects match the representation of anatomy in the atlas. While registration can bring the individual into correspondence with the atlas, and a common coordinate system enables the pooling of activation data and multi-subject comparisons, the accuracy and utility of the atlas is equally dependent on the anatomical template itself [33]. The Talairach templates were based on post mortem sections of a 60 year-old female subject's brain, which clearly did not reflect the *in vivo* anatomy of subjects in activation studies. The atlas plates were also compromised by a variable slice separation (3-4 mm), and data from orthogonal planes were inconsistent. To address these limitations, a composite MRI dataset was constructed from several hundred young normal subjects (239 males, 66 females; age: 23.4 ± 4.1 y) whose scans were individually registered into the Talairach system by linear transformation, intensity normalized, and averaged on a voxel-by-voxel basis [34,35]. Although the resulting average brain has regions where individual structures are blurred due to spatial variability in the population [34,35], the effect of anatomical variability in different brain areas is illustrated qualitatively by this map. Meanwhile, automated methods were rapidly being developed to register new MRI and PET data into a common space (see [36,37], for a comparative study and a review). These algorithms could be used to optimally align new MR data with the template by maximizing a measure of intensity similarity, such as 3D cross-correlation [38-40], ratio image uniformity [41], or mutual information [42-45]. Mutual information has also been shown to be a powerful registration metric when there is only a statistical dependency, rather than a direct linear relation, between the intensities of the images being aligned [43]. Any alignment transformation defined for one modality, such as MRI, can be identically applied to another modality, such as PET, if a previous cross-modality intrasubject registration has been

performed [46]. For the first time then, PET data could be mapped into stereotaxic space via a correlated MR dataset [35,46]. Registration algorithms therefore made it feasible to automatically map data from a variety of modalities (such as those in Fig. 1) into an atlas coordinate space based directly on the Talairach reference system.

5. Deformable brain atlases

Anatomic variability

The use of spatial normalization schemes based upon deep white matter features (the AC and PC), such as outlined above, will never completely accommodate the most variable of brain structures, the cortex. The cortex is also the site of interest for most functional activation studies. Considerable normal variation in sulcal geometry are well-documented in primary motor, somatosensory and auditory cortex [47,48], primary and association visual cortex [49], frontal and pre-frontal areas [50], and lateral perisylvian cortex [8,51-53]. More recent 3D analyses of anatomic variability, based on post mortem and normal and diseased populations *in vivo*, have found a highly heterogeneous pattern of anatomic variation [54-56, 94]. Fig. 2 shows average anatomical maps of the lateral ventricles, based on averaging surface models from 10 patients with Alzheimer's disease and 10 demographically matched control subjects. The color code shows heterogeneous profiles of variability across the ventricles. Still greater variability is apparent in Fig. 3, when surface models of the cortical sulci are compared. This variability is so great that anatomical models must often be averaged across subjects to identify typical patterns of asymmetry, variability, and displacement within and between groups.

Given this complex structural variability between normal individuals, and particularly between different populations (healthy and diseased), a fixed brain atlas may fail to serve as a faithful representation of every brain [21,33]. Since no two brains are the same, this presents a challenge for attempts to create standardized atlases. Even in the absence of any pathology, brain structures vary between individuals in every metric; shape, size, position and orientation relative to each other. Such normal variations have complicated the goals of comparing functional and anatomic data from many subjects [33,48].

Numerous studies have measured how severe the inter subject variations in anatomy are, even after transforming individual anatomic data into the Talairach stereotaxic system (Figs. 2 and 3). Clearly, direct averaging of digital brain maps, after transformation to a common 3D coordinate space, is only valid if homologous cortical regions in different subjects have been brought into register by the registration transform. The most severe challenge occurs when the topology itself is undergoing considerable dynamic change due to development or degeneration, for example. Direct digital subtraction of stereotaxic functional maps in studies of diseases (such as dementia) may lead to spurious results: maps of apparent significance may reflect differences which are anatomic, rather than functional, in character [57,58]. These difficulties have led to the suggestion that direct reference to the sulci that frame architectonic fields may present a more reliable basis for functional mapping than reference to a single standard or idealized brain [48,53,54,56,59,94].

6. Warping

The fact that the Talairach brain fails to match individual scans stems partly from two facts. First, Talairach registration is only based on linear transformations (rotation, scaling, translation). Second, the origin of the coordinate system was selected to solve mapping and localization problems deep in the brain where individual variability is relatively low.

Atlases can be greatly improved if they are elastically deformed to fit a new image set from an incoming subject. Local warping transformations (including local dilations, contractions and shearing) can adapt the shape of a digital atlas to reflect the anatomy of an individual subject, producing an individualized brain atlas. Fig. 4 shows a deformable cryosection atlas, which is adapted using surface-based elastic warping to match the anatomy of an individual patient [94]. Introduced by Bajcsy and colleagues at the University of Pennsylvania [60-63], this approach was adopted by the Karolinska Brain Atlas Program [24,28,64], where warping transformations are applied to a digital cryosection atlas to adapt it to individual CT or MR data and co-registered functional scans.

Image warping algorithms, specifically designed to handle 3D neuroanatomic data [38,40, 65-77] can transfer all the information in a 3D digital brain atlas onto the scan of any given subject, while respecting the intricate patterns of structural variation in their anatomy. These transformations must allow any segment of the atlas anatomy to grow, shrink, twist and rotate, to produce a transformation that encodes local differences in topography from one individual to another. Deformable atlases [24,25,62,65,78-81] resulting from these transformations can carry 3D maps of functional and vascular territories into the coordinate system of different subjects. The transformations also can be used to equate information on different tissue types, boundaries of cytoarchitectonic fields and their neurochemical composition.

Warping algorithms calculate a 3D deformation field which can be used to non-linearly register one brain with another (or with a neuroanatomic atlas). The resultant deformation fields can subsequently be used to transfer physiologic data from different individuals to a single anatomic template. Functional data from different subjects can then be compared and integrated in a context where confounding effects of anatomical shape differences are factored out. Non-linear registration algorithms therefore support the integration of multi-subject brain data in a stereotaxic framework, and are increasingly used in functional image analysis packages [24, 82].

Any successful warping transform for cross-subject registration of brain data must be high-dimensional, to accommodate fine anatomic variations [66,83]. This warping is required to bring the atlas anatomy into structural correspondence with the target scan at a very local level. Another difficulty arises from the fact that the topology and connectivity of the deforming atlas have to be maintained under these complex transforms. This is difficult to achieve in traditional image warping manipulations [84,85]. Physical continuum models of the deformation address these difficulties by considering the deforming atlas image to be embedded in a 3D deformable medium, which can be either an elastic material or a viscous fluid. The medium is subjected to certain distributed internal forces, which reconfigure the medium and eventually lead the image to match the target. These forces can be based mathematically on the local intensity patterns in the datasets, with local forces designed to match image regions of similar intensity.

Model-driven registration

To guide the mapping of an atlas onto an individual, higher-level structural information can be invoked to guarantee the biological validity of the resulting transform [69,70,83,86,87]. In one approach [70] anatomic surfaces, curves and points are extracted (with a combination of automatic and manual methods), and forced to match. Fig. 5 illustrates this approach in 2D, where stained histologic sections are elastically reconfigured into their original morphology in the cryosection blockface [83]. In 3D, the procedure calculates the volumetric warp of one brain image into the shape of another, by calculating the deformation field required to elastically transform functionally important surfaces in one brain into precise structural correspondence with their counterparts in a target brain. This transformation is illustrated in Fig. 4. The scheme involves the determination of several model surfaces, a warp between these surfaces, and the construction of a volumetric warp from the surface warp [56].

Model-driven warping algorithms perform well when warping neuroanatomic data not only between subjects but also between modalities. This presents new opportunities to transfer cytoarchitectural and neurochemical maps from high-resolution 3D cryosection data [88] onto in vivo functional scans, and digitally correlate the resulting maps within a stereotaxic atlas space. Recent studies have used deformable registration to correlate histologic markers of Alzheimer's disease with metabolic PET signals in vivo, while correcting for tissue deformation due to post mortem changes and histologic processing [22] (Fig. 5). Deformable atlas approaches offer a powerful means to transfer multimodal 3D maps of functional and neurochemical territories between individuals and neuroanatomic atlases, respecting complex differences in the topography of the cortex and deep anatomic systems. These algorithms can also be applied to high-resolution brain atlases based on 3D digital cryosection images, to produce flexible high-resolution templates of neuroanatomy that can be adapted to reflect individual subjects' anatomy [88-90].

Automated deformable atlases promise to have considerable impact on clinical and research imaging applications. Atlas deformations can carry pre-segmented digital anatomic models, defined in atlas space, into new patients' scans, automatically labeling their anatomy [40]. Non-linear registration of 3D geometric atlases onto individual datasets has been used to support automated brain structure labeling for hippocampal morphometry [91], analysis of subcortical structure volumes in schizophrenia [92], estimation of structural variation in normal and diseased populations [38,39,93,94], and segmentation and classification of multiple sclerosis lesions [95]. Projection of digital anatomic models into PET data can also serve to define regions of interest for quantitative calculations of regional cerebral blood flow [28].

7. Encoding structural variability in human populations

Deformable registration algorithms produce extremely detailed 3D maps of regional differences that can be used to investigate dynamic structure alterations in disease or brain development. The complex profiles of dilation and contraction required to warp a digital atlas onto a new subject's brain provide an index of the anatomical shape differences between that subject's brain and the atlas [69,96-99]. Atlas deformation maps offer a framework for pathology detection [83,93,94,97,100], identification of gender-specific anatomic patterns [69,86], and mapping of dynamic patterns of structural change in neurodevelopmental and degenerative disease processes [23,101,141].

As noted earlier, due to pronounced anatomic variability between individual human brains, any atlas or clinical diagnostic system based on a single subject's anatomy cannot succeed fully. A deformable brain atlas counteracts some of the limitations of a fixed atlas by using mathematically flexible transformations. Nonetheless, its success is still based on the premise that brains resemble a prototypical template of anatomy, and can be produced by continuously deforming it.

Atlasing considerations suggest that a statistical confidence limit, rather than an absolute representation of neuroanatomy, may be more appropriate for representing particular subpopulations. Methods to create probabilistic brain atlases currently fall into three major categories, each differing slightly in its conceptual foundations. The three methods are: intensity-based, label-based, and deformation-based approaches.

1. Intensity-based approaches

Initial approaches to population-based atlasing concentrated on generating average representations of anatomy by intensity averaging of multiple MRI scans [34,102]. The average that results has large areas, especially at the cortex, where individual structures are blurred due to spatial variability in the population. Fig. 6 shows typical cross-sections from this average

intensity dataset. Because the gyral patterns are not locally registered, the resulting average brain also tends to exceed the average dimensions of the component brain images. The templates can, however, be used as targets for automated registration, and assist in mapping MR and co-registered functional data into stereotaxic space [35].

Since intensity averaging after linear registration washes away the gyral features of the cortex (Fig. 6), higher-order registration can be used to produce a better-resolved template. By averaging geometric and intensity features separately (cf. [23,56,97,100,103]), a template can be made with the mean intensity and geometry for a specific population. Briefly, an initial image template for the group is constructed by: (1) using automated linear transformations [46] to align the MRI data with a randomly selected image; (2) intensity-averaging the aligned scans; and then (3) recursively re-registering the scans to the resulting average affine image. The resulting average image is then adjusted to have the mean affine shape for the group [74]. This step defines the global shape of the template, and uses matrix exponentiation to define average transformations. Briefly, at each round of registrations, all affine transformations mapping individuals to the current registration target are collected, and the arithmetic mean of their matrix logarithms is computed; using matrix exponentiation, an average transformation is recovered. By concatenating the inverse of this transform with the individual transforms, each individual image can be transformed into register with the others, while assuming the average global shape and scale for the group. At each pass of this procedure, which takes several iterations, intensities of the aligned scans are averaged voxel-by-voxel.

After this initial affine alignment, surface-based elastic transformations, with millions of degrees of freedom, can be used to reconfigure each subject's 3D image into the average anatomic configuration for the group. Note that if non-linear registration were being used to align every scan to a single individual image, there would not be any average geometry, but just the geometry of the target image. Instead, surface-based non-linear registration is used to align each scan with an average set of anatomical models. Unlike in the case of intensity-based registration, there are no intensities in the target scan, just an average set of models. These models define the average geometry for the group, for a wide range of anatomic systems. Because every scan is mapped into exact structural registration with this set of average models, the resulting average image (and in fact the individual reconfigured images) have the average regional geometry for the group.

By averaging the reconfigured images (after intensity normalization), a group average image is created with: (1) the mean global geometry [74]; (2) the mean regional geometry [23]; and (3) the mean image intensity for the group. This final step produces a crisp image template to represent the average anatomy of the group (Fig. 6). Note the better-resolved cortical features in the average images after high-dimensional cortical registration. By explicitly computing matching fields that relate gyral patterns across subjects, a well-resolved and spatially consistent set of probabilistic anatomical models and average images can be made to represent the average anatomy and its variation in a subpopulation [56]. These high-dimensional brain templates can serve as the foundation for population-based disease-specific atlases (e.g. Fig. 1; [23,104-107]).

2. Label-based approaches

In label-based approaches ([35]; also known as SPAM approaches, short for statistical/probabilistic anatomy maps), large ensembles of brain data are manually labeled, or 'segmented', into sub-volumes, after registration into stereotaxic space. A probability map is then constructed for each segmented structure, by determining the proportion of subjects assigned a given anatomic label at each voxel position [35,108,109]. The information which these probability maps provide on the location of various tissue classes in stereotaxic space has been useful in designing automated tissue classifiers and approaches to correct

radiofrequency and intensity inhomogeneities in MR scans [110]. In our laboratory, we have also used SPAM probabilistic maps to constrain the search space for significant activations in PET and SPECT imaging experiments [111,112], and to detect regional patterns of gray matter loss during late brain development [113].

3. Deformation-based approaches

As noted earlier, when applied to two different 3D brain scans, a non-linear registration calculates a deformation map (Figs. 5 and 7) that matches brain structures in one scan with their counterparts in the other. In probabilistic atlases based on deformation maps [83,93,94, 99], statistical properties of these deformation maps are encoded locally to determine the magnitude and directional biases of anatomic variation. Fig. 7 shows a computational approach which measures differences in cortical patterning using complex shape deformations ([23,54, 55,93,94]; see next section for details). Encoding of local variation can then be used to assess the severity of structural variants outside of the normal range, which may be a sign of disease ([93,94]; see Section 9). A major goal in designing this type of pathology detection system is to recognize that both the magnitude and local directional biases of structural variability in the brain may be different at every single anatomic point [54,55]. In contrast to the intensity averaging of other current approaches [34,102], an anisotropic random vector field framework is introduced to encode directional biases in anatomic variability and map out abnormalities in new subjects [93,94].

The three major approaches for probabilistic atlas construction differ only in the attribute whose statistical distribution is modeled and analyzed. Random vector fields (i.e. vector distributions of deformation vectors at each point in space) are analyzed in approaches based on deformation maps, while random scalar fields are used to model MR intensity statistics in the density-based approach, and to model the incidence of binary labels in space in the label-based approach.

8. Registration of cortical patterns

Cortical morphology is notoriously complex, and presents unique challenges in anatomic modeling investigations. In response to these challenges, much research has been devoted to developing cortical parameterization and flattening algorithms. These methods optimally transform maps of cortical features onto a simpler, non-convoluted surface such as a 2D plane [114-117,135], an ellipsoid [118,119] or a sphere [54,56,69,86,93,94,120]. Fig. 7 shows examples of these types of maps, with color fields imposed [99] to retain 3D information on cortical geometry.

Warping the cerebral cortex

Despite the advantages provided by transformations that simplify its geometry, the cortical surface presents challenges for all registration algorithms that strive to match the anatomy of one subject with another. The need to make comparative measurements at the cortex across subjects requires a surface-to-surface warp which not only matches overall cortical geometry, but also enforces point-to-point correspondence to a higher degree. Specialized approaches have been developed to match cortical regions, so that networks of sulci and gyri are individually matched (Fig. 7; [70,83]). Unfortunately, differences in the serial organization of cortical gyri prevent exact gyrus-by-gyrus matching of one cortex with another. Some cortical areas are particularly subject to variations in the incidence and topology of accessory gyri, and one subject may have two or three gyri where one gyrus is found in another subject. This feature is especially notable in studies of paracingulate and temporo-parietal regions, in particular the planum temporale and posterior perisylvian areas which form a critical part of the language representation of the left hemisphere [8,109,121]. Nonetheless, an important intermediate goal in cortical registration has been to match a comprehensive network of sulcal and gyral elements

that are consistent in their incidence and topology across subjects ([8,121]; see Appendix A for details).

Metrical adjustments

In cortical registration, planar (or spherical) maps serve as proxies for the cortex, easing the computation of the surface mappings (Fig. 7). However, different amounts of local dilation and contraction are required to transform the cortex onto these simpler 2-parameter surfaces. In the covariant tensor approach [83], exact information on these metric alterations is stored in the metric tensor of the mapping, $g_{jk}(\mathbf{r})$. In the subsequent matching procedure, correction terms (Christoffel symbols, Γ^i_{jk}) make the necessary adjustments for fluctuations in the metric tensor of the mapping procedure. Since metric distortions caused by mappings to spheres or planes can always be encoded as a metric tensor field, a covariant approach supports comparisons of cortical data using either flattened or spherical maps. In the partial differential equation formulation (1), we replace L by the covariant differential operator L^\ddagger . In L^\ddagger , all L 's partial derivatives are replaced with covariant derivatives. These covariant derivatives are defined with respect to the metric tensor of the surface domain where calculations are performed (see Appendix A). With this mathematical adjustment, we eliminate the confounding effects of metric distortions that necessarily occur during the mapping procedure. The resulting cortical matching field is independent of the auxiliary mappings (spherical or planar) used to extract it.

Retention of 3D cortical information

To ensure that each subject's spherical map can be converted back into a 3D cortical model, cortical surface point position vectors in 3D stereotaxic space are represented on the sphere using a color-code (at 16 bits per channel). This forms an image of the parameter space in RGB color image format (Figs. 7 and 8; [99]). To find good matches between cortical regions in different subjects, we first derive a color image map for each respective surface model, and transfer the entire network of sulcal curves back onto it. After performing the matching process using a flow in the parametric space (Fig. 7), the corresponding 3D mapping is recovered, carrying one cortex onto another.

Alignment of cortical patterns

Fig. 8 shows the appearance of the maps in the software used to perform the alignment of cortical patterns. Both Fig. 8(c) and (d) show a color field representing cortical positions for the same subject, but in Fig. 8(d) this color field has been warped so that curved anatomic features in this individual occur at pre-defined parameter locations in the parameter space. These locations are defined to be the average parameter locations for the group at which this curved feature occurs. In other words, color maps represent the 3D cortical geometry of each individual. When these color maps are warped (Fig. 8(d)), they still represent the same cortical geometry (Fig. 8(f)) of that same individual, but the parameter locations that index given anatomical landmarks in the folded brain surface have been adjusted. The adjustment assigns to each landmark in the folded brain surface a parameter pair that is consistent across subjects. By doing this, corresponding cortical features can be accessed in each subject by referring to the adjusted parametric coordinates. Note that the initial color field (Fig. 8(c)) for the individual subject is much smoother than the warped color field (Fig. 8(d)), because the initial surface parameterization (Fig. 8(c) and (e)) corresponds to the minimum energy configuration of a deformable surface, which tends to equalize the edge lengths and size of the surface tiles (Fig. 8(e); [122]). The adjusted parameterization (Fig. 8(f)) is less smooth, i.e. its spatial derivatives are more variable, since there are additional anatomic constraints on the parameterization. Nonetheless, a minimally distorted parameterization can still be obtained by defining a covariant differential operator or a variational measure of distortion (see Appendix A). The

parameterization that minimizes this distortion measure, while enforcing the anatomic boundary conditions, can be obtained as the solution to the associated system of partial differential equations (see Appendix A, and [23,104]).

Note that the parameter space can be displayed in planar format for easier manipulation. In practice, corresponding 3D models are recovered from the warped color maps (Fig. 8(e) and (f)) allowing the user to confirm that the surface mesh has adapted accurately to anatomical landmarks in different subjects.

9. Cortical averaging

The warping field deforming one cortex into gyral correspondence with another can also be used to create an average model of the cortex. To do this, all 36 gyral curves for all subjects are first transferred to the spherical parameter space. Next, each curve is uniformly re-parameterized to produce a regular curve of 100 points on the sphere whose corresponding 3D locations are uniformly spaced. A set of 36 average gyral curves for the group is created by vector averaging all point locations on each curve. This average curve template (curves in Fig. 8(b)) serves as the target for alignment of individual cortical patterns (cf. [120]). Each individual cortical pattern is transformed into the average curve configuration using a flow field within the spherical map (Fig. 8(a) and (b); cf. [123]). By carrying a color code (that indexes 3D locations) along with the vector flow that aligns each individual with the average folding pattern, information can be recovered at a particular location in the average folding pattern (Fig. 8(d)) specifying the 3D cortical points mapping each subject to the average. This produces a new coordinate grid on a given subject's cortex (Fig. 8(f)) in which particular grid-points appear in the same location across subjects relative to the mean gyral pattern. By averaging these 3D positions across subjects, an average 3D cortical model can be constructed for the group. An example of this type of cortical average, based on nine cognitively matched subjects with Alzheimer's disease, is shown in Fig. 9 (bottom row; [23]). The resulting mapping is guaranteed to average together all points falling on the same cortical locations across the set of brains, and ensures that corresponding features are averaged together.

Cortical variability

By using the color code (Fig. 7(d)) to identify original cortical locations in 3D space (Fig. 7(f)), displacement fields can be recovered mapping each patient into gyrus-by-gyrus correspondence with the average cortex. Fig. 10 shows an example of this type of displacement field. Anatomic variability is then defined at each point on the average cortex as the root mean square (r.m.s.) magnitude of the 3D displacement vectors, assigned to each point, in the surface maps driving individuals onto the group average [54-56,93,94]. A typical variability pattern (based on 26 subjects) is visualized as a color-coded map in Fig. 11 [23].

Overall, variability values rise sharply (Fig. 11) from 4-5 mm in primary motor cortex to localized peaks of maximal variability in posterior perisylvian zones and superior frontal association cortex (16-18 mm). The region of maximal variability, in temporal cortex, is tightly linked with the location of human visual area MT (or V5; [59]). This suggests that extreme caution is necessary when referring to activation foci in this important area using stereotaxic coordinates, unless a non-linear registration approach is employed. The overall patterns of variation corroborate recent volumetric findings based on a fine-scale parcellation of the cortex [124], and suggest a greater morphologic individuality in cortical regions that are phylogenetically more recent.

Tensor maps of directional variation

Structures do not vary to the same degree in every coordinate direction [55], and even these directional biases vary by cortical system. The principal directions of anatomic variability in a group can be shown in a tensor map (Figs. 12 and 13). The maps have two uses. First, they make it easier to detect anomalies, which may be small in magnitude but in an unusual direction (see Section 9). Second, they significantly increase the information content of Bayesian priors used for automated structure extraction and identification [63,125,126,139].

Fig. 12 shows a tensor map of variability for normal subjects, after mapping 20 elderly subjects' data into Talairach space (all right handed, 10 males, 10 females). Rectangular glyphs indicate the principal directions of variation—they are most elongated along directions where anatomic variation is greatest across subjects. Each glyph represents the quadratic form determined by the covariance tensor of the vector fields that map individual subjects onto their group average [93,142]. Because gyral patterns constrain the mappings, the fields reflect variations in cortical organization at a more local level than can be achieved by only matching global cortical geometry. Note the elongated glyphs in anterior temporal cortex, and the very low variability (in any direction) in entorhinal and inferior frontal areas. By better defining the parameters of allowable normal variations, the resulting information can be leveraged to distinguish normal from abnormal anatomical variants [93,94,127].

10. Pathology detection

In a probabilistic atlas, well-defined statistical criteria are required to identify significant differences in brain structure. These criteria can be formulated in different ways, depending on the attribute whose statistical variation is modeled. One approach is to use the theory of Gaussian random fields, a modeling technique used widely in functional image analysis (e.g. SPM; [82]). By contrast with functional signals, which are generally treated as random scalar fields, the deformation maps that quantify structural differences are treated as random vector fields. Instead of a field of variance values, the variability of the deformation vectors, and their directional tendencies, are stored using a covariance tensor at each anatomical point [55, 128].

In one study (cf. [93,94,128]), we developed an approach to detect brain structure differences between two groups, or between an individual subject and a database of demographically matched subjects. Suppose $\mathbf{W}_{ij}(\mathbf{x})$ is the deformation vector required to match the structure at position \mathbf{x} in an atlas template with its counterpart in subject i of group j . (If surface models are being analyzed, rather than full brain volumes [83], $\mathbf{W}_{ij}(\mathbf{x})$ is the deformation vector matching parametric mesh node $\mathbf{x}(u,v)$ with its counterpart in subject i of group j .) We then model the deformations as:

$$\mathbf{W}_{ij}(\mathbf{x}) = \mu_j(\mathbf{x}) + \Sigma(\mathbf{x})^{1/2} \epsilon_{ij}(\mathbf{x}). \quad (1)$$

Here $\mu_j(\mathbf{x})$ is the mean deformation for group j , and $\Sigma(\mathbf{x})$ is a non-stationary, anisotropic covariance tensor field (Fig. 13), which relaxes the confidence threshold for detecting abnormal structure in regions where normal variability is extreme, $\Sigma(\mathbf{x})^{1/2}$ is the upper triangular Cholesky factor tensor field, and $\epsilon_{ij}(\mathbf{x})$ is a trivariate random vector field whose components are independent stationary Gaussian random fields.

Deformation-based morphometry

A T^2 or F statistic that indicates evidence of significant difference in deformations between the groups is calculated at each lattice location in a 3D image or parameterized 3D surface, to form a statistic image [93,94]. Under the null hypothesis of no abnormal deformations, the

statistic image is approximated by a T^2 random field. Specifically, the significance of a difference in brain structure between two subject groups (e.g. patients and controls) of N_1 and N_2 subjects is assessed by calculating the sample mean and variance of the deformation fields ($j = 1, 2$):

$$\begin{aligned} \mathbf{W}_j^\mu(\mathbf{x}) &= \sum_{i=1}^{N_j} \mathbf{W}_{ij}(\mathbf{x}) / N_j \\ \psi(\mathbf{x}) &= (1 / (N_1 + N_2 - 2)) \times \left\{ \sum_{j=1}^2 \sum_{i=1}^{N_j} [\mathbf{W}_{ij}(\mathbf{x}) - \mathbf{W}_j^\mu(\mathbf{x})] [\mathbf{W}_{ij}(\mathbf{x}) - \mathbf{W}_j^\mu(\mathbf{x})]^T \right\}. \end{aligned} \quad (2)$$

and computing the following statistical map [93,94,128]:

$$T^2(\mathbf{x}) = \{N_1 N_2 / (N_1 + N_2)(N_1 + N_2 - 2)\} [\mathbf{W}_2^\mu(\mathbf{x}) - \mathbf{W}_1^\mu(\mathbf{x})]^T \times [\psi(\mathbf{x})]^{-1} [\mathbf{W}_2^\mu(\mathbf{x}) - \mathbf{W}_1^\mu(\mathbf{x})]. \quad (3)$$

Under the null hypothesis, $(N_1 + N_2 - 2) T^2(\mathbf{x})$ is a stationary Hotelling's T^2 -distributed random field. At each point, if we let $v = (N_1 + N_2 - 2)$ and we let the dimension of the search space be $d = 3$, then:

$$F(\mathbf{x}) = ((v - d + 1) / d) T^2(\mathbf{x}) \sim F_{d,(v-d+1)}. \quad (4)$$

In other words, the field can be transformed point-wise to a Fisher-Snedecor F distribution [93,94]. To obtain a p -value for the effect that is adjusted for the multiple comparisons involved in assessing a whole field of statistics, [128] examined the distribution of the global maximum T_{\max}^2 of the resulting T^2 -distributed random field under the null hypothesis. The resulting probability that $T^2(\mathbf{x})$ ever exceeds a fixed high threshold T_{\max}^2 is approximated by the expected Euler characteristic $E[\chi(A(T_{\max}^2))]$ of the excursion sets of the Hotelling's T^2 -distributed random field above the threshold T_{\max}^2 . Then $p[T_{\max}^2 \geq t]$ is approximated by $\sum_{n=0}^d R_n \rho_n(t)$ where the number of n -dimensional resolution elements $R_n = V_n / (\text{FWHM})^n$ depends on the effective full-width-at-half-max (FWHM) of the component Gaussian images $\epsilon_{ij}(\mathbf{x})$, and on the Euler characteristic (V_0), caliper diameter ($V_1/2$), surface area ($2V_2$) and volume (V_3) of the search region. The n -dimensional EC densities are given by [128]:

$$\begin{aligned} \rho_0(t) &= \int_t^\infty \frac{\Gamma(\frac{v+1}{2})}{\Gamma(\frac{3}{2})\Gamma(\frac{v-2}{2})} \left[1 + \frac{u}{v}\right]^{-(v+1)/2} \frac{u^{1/2}}{v^{3/2}} du, \\ \rho_1(t) &= \frac{(4 - \ln 2)^{1/2} \Gamma(\frac{v+1}{2})}{\pi^{1/2} \Gamma(\frac{3}{2}) \Gamma(\frac{v-1}{2})} \left[1 + \frac{t}{v}\right]^{-(v-1)/2} \frac{t}{v}, \\ \rho_2(t) &= \frac{4 - \ln 2}{\pi} \frac{\Gamma(\frac{v+1}{2})}{\Gamma(\frac{3}{2})\Gamma(\frac{v-2}{2})} \left[1 + \frac{t}{v}\right]^{-(v-1)/2} \times \left(\frac{t}{v}\right)^{1/2} \left(\frac{t}{v} - \frac{2}{v-2}\right), \quad \text{and} \\ \rho_3(t) &= \frac{(4 - \ln 2)^{3/2}}{\pi^{3/2}} \frac{\Gamma(\frac{v+1}{2})}{\Gamma(\frac{3}{2})\Gamma(\frac{v-3}{2})} \left[1 + \frac{t}{v}\right]^{-(v-1)/2} \times \left(\left(\frac{t}{v}\right)^2 + \frac{5}{v-3} \frac{t}{v} + \frac{2}{(v-1)(v-3)}\right) \end{aligned} \quad (5)$$

The global maximum of the random deformation field, or derived tensor fields [23,94], can be used to test the hypothesis of no structural change in disease [128]. Similar multivariate linear models can be used to test for the effect of explanatory variables (e.g. age, gender, clinical test scores) on a set of deformation field images [129,130]. This can help explore linkages between atlas descriptions of variance and behavioral, cognitive, or genetic parameters [111,131,132, 137].

Pattern-theoretic approaches

In a related approach based on pattern theory [100], deformation maps expressing variations in normal anatomies are calculated with a non-linear registration procedure based on continuum mechanics [65,78]. Each deformation map is expanded in terms of the eigenfunctions of the governing operator that controls the transformations (such as the Laplacian ∇^2 [73] or Cauchy-Navier operator $(\lambda + \mu)\nabla(\nabla \cdot) + \mu\nabla^2$ [66]). Gaussian probability measures are defined on the resulting sequences of expansion coefficients [100,133]. Essentially this spectral formulation is a model of anatomic variability. Once the model parameters σ_k are learned (see Remark 1), every subject's anatomy can be represented by a feature vector (z_1, \dots, z_n) , whose elements are just the coefficients of the deformation field required to match their particular anatomy with a mean anatomical template. If the parameters of anatomical variation are altered in disease, a pattern classifier can classify new subjects according to their statistical distance from the diseased group mean relative to the normal group mean [93,94,134]. Currently being tested as a framework to encode anatomic variation, these deformable atlas systems show considerable promise in identifying disease-specific differences [91,134]. Bayesian algorithms for automated identification of brain structures, which include approaches based on deformable image registration, can benefit greatly from encoded information on anatomic variability [100,126,129,135,138].

Remark 1—In Grenander's formalism [100], the distribution of the random deformation fields $\mathbf{u}(\mathbf{x})$ is assumed to satisfy the stochastic differential equation:

$$L(\mathbf{u}(\mathbf{x})) = \mathbf{e}(\mathbf{x}). \quad (6)$$

Here L is the operator governing the deformation and $\mathbf{e}(\mathbf{x})$ is a 3×1 random noise vector field, whose coefficients in L 's eigenbasis are zero-mean independent Gaussian variables with variances σ_k^2 . If the differential operator L has eigenbasis $\{\phi_k^{(x)}\}$ with eigenvalues $\{\lambda_k\}$, a probability density can be defined directly on the deformation field's expansion coefficients (z_1, \dots, z_n) . If

$$\mathbf{u}(\mathbf{x}) = \sum_k z_k \phi_k(\mathbf{x}) \quad (7)$$

then:

$$p(z_1, \dots, z_n) = \exp \left[-\frac{1}{2} \left(\sum_{k=1}^n \log \left\{ 2\pi\sigma_k^2/\lambda_k^2 \right\} + \left(\sum_{k=1}^n |\lambda_k z_k|^2 / \sigma_k^2 \right) \right) \right]. \quad (8)$$

11. Conclusion

As we have seen, the essential requirement for the construction and use of atlases is registration. Registration enables atlases to measure, visualize, compare and summarize brain images. An atlas can take on many forms, from descriptions of structure or function of the whole brain to maps of groups or populations (Fig. 1). Individual systems of the brain can be mapped as can relationships between subjects, modalities and attributes. Differences between species can even be catalogued. But in most cases, the value added by registered brain atlases is the unique and critical ability to integrate information from multiple sources. The utility of an atlas is dependent upon appropriate coordinate systems, registration and deformation methods along

with useful visualization strategies. Accurate and representative atlases of brain hold enormous promise for helping to create a comprehensive understanding of brain in health and disease.

Acknowledgments

The authors are grateful to the faculty and staff of the Laboratory of Neuro Imaging who contributed directly or indirectly to the work described in this chapter. The scientific investigations that form the basis for this work were supported by research grants from the National Library of Medicine (LM/MH05639), the National Science Foundation (BIR 93-22434), the National Center for Research Resources (RR05956 and P41 RR13642), the National Institute of Neurological Disorders and Stroke and the National Institute of Mental Health NINDS/NIMH (NS38753), and by a Human Brain Project grant known as the International Consortium for Brain Mapping, which is funded jointly by NIMH and NIDA (P20 MH/DA52176).

Appendix A

A.1. 3D Matching of cortical surfaces

Differences in cortical patterning across subjects can be computed by using a deformation algorithm to match cortical surfaces across subjects. Our method [23,70,93,94] is conceptually similar to those of Dale and Sereno [69], Davatzikos [118], and Fischl et al. [120]. 3D active surfaces [143] extract parametric representations of each subject's cortex, by deforming a tiled spherical mesh into the shape of the cortex. On these surface models, corresponding networks of anatomical curves are identified. Specifically, 36 parametric curves are created per subject to represent the major elements of the gyral pattern. These include the superior and inferior frontal, central, postcentral, intraparietal, superior and inferior temporal, collateral, olfactory and occipito-temporal sulci, as well as the Sylvian fissures. Additional 3D curves are drawn in each hemisphere to represent gyral limits at the interhemispheric margin [93,94]. Stereotaxic locations of contour points derived from the data volume are then redigitized to produce 36 uniformly parameterized cortical contours per brain, representing the primary gyral pattern of each subject [93,94]. The transformation relating these networks is expressed as a vector flow field in the parameter space of the cortex (Fig. 7). This vector flow field in parameter space indirectly specifies a correspondence field in 3D, which drives one cortical surface into the shape of another. This mapping not only matches overall cortical geometry, but matches the entire network of the 36 landmark curves with their counterparts in the target brain, and thus is a valid encoding of cortical variation.

Spherical, planar maps of cortex

Several simpler maps of the cortex are made to help calculate the transformation. Because each subject's cortical model is arrived at by deforming a spherical mesh [69,70,122], any point on the cortex maps to exactly one point on the sphere, and a spherical map of the cortex is made which indexes sulcal landmarks in the normally folded brain surface. These spherical locations, indexed by two parameters, can also be mapped to a plane (Fig. 7; [83,93,94]). A flow field is then calculated that elastically warps one flat map onto the other (Fig. 8; or equivalently, one spherical map to the other). On the sphere, the parameter shift function $\mathbf{u}(\mathbf{r}): \Omega \rightarrow \Omega$, is given by the solution $F_{pq}: \mathbf{r} \rightarrow \mathbf{r} - \mathbf{u}(\mathbf{r})$ to a curve-driven warp in the spherical parametric space $\Omega = [0, 2\pi] \times [0, \pi]$ of the cortex [55,94]. For points $\mathbf{r} = (r, s)$ in the parameter space, a system of simultaneous partial differential equations can be written for the flow field $\mathbf{u}(\mathbf{r})$:

$$\begin{aligned} L^\ddagger(\mathbf{u}(\mathbf{r})) + \mathbf{F}(\mathbf{r} - \mathbf{u}(\mathbf{r})) &= 0, \quad \forall \mathbf{r} \in \Omega, \\ \mathbf{u}(\mathbf{r}) &= \mathbf{u}_0(\mathbf{r}), \quad \forall \mathbf{r} \in M_0 \cup M_1. \end{aligned} \tag{A1}$$

Here M_0, M_1 are sets of points and (sulcal or gyral) curves where displacement vectors $\mathbf{u}(\mathbf{r}) = \mathbf{u}_0(\mathbf{r})$ matching corresponding anatomy across subjects known. The flow behavior is modeled

using equations derived from continuum mechanics, and these equations are governed by the Cauchy-Navier differential operator $L = \mu\nabla^2 + (\lambda + \mu)\nabla(\nabla^T \cdot)$ with body force \mathbf{F} [55,56,94, 100]. The only difference is that L^\dagger is the covariant form of the differential operator L , for reasons explained in the next section.

Covariant field equations

Since the cortex is not a developable surface [69,86], it cannot be given a parameterization whose metric tensor is uniform. As in fluid dynamics or general relativity applications, the intrinsic curvature of the solution domain should be taken into account when computing flow vector fields in the cortical parameter space, and mapping one mesh surface onto another; otherwise errors will arise. The result is a covariant regularization approach [56,83,144]. From a practical standpoint, this approach uses a mathematical trick that makes it immaterial whether a spherical or planar map is used to simplify the mathematics of cortical matching. Either a spherical or a planar map can be used. Since the flows defined on these maps are adjusted for variations in the metric tensor of the mapping, the results become independent of the underlying parameterization (spherical or planar). In fact, spherical and planar maps involve different amounts of local dilation or contraction of the surface metric, but this metric tensor field is stored and used later to adjust the flow that maps one cortex on another, so which one is used is immaterial. The covariant approach was introduced by Einstein [144] to allow the solution of physical field equations defined by elliptic operators on manifolds with intrinsic curvature. Similarly, the problem of deforming one cortex onto another involves solving a similar system of elliptic partial differential equations [69,83,116,123], defined on an intrinsically curved computational mesh (in the shape of the cortex). In the covariant formalism, the differential operators governing the mapping of one cortex to another are adaptively modified to reflect changes in the underlying metric tensor of the surface parameterizations (Fig. 7). These equations are formulated using covariant derivatives (described next), which allow a PDE to be run on a manifold whose Riemann curvature tensor is non-zero.

Covariant derivatives

The covariant derivative of a (contravariant) vector field, $u^i(\mathbf{x})$, is defined as:

$$u_{,k}^i = \partial u^j / \partial x^k + \Gamma_{ik}^j u^i \quad (A2)$$

[83] where the Γ_{ik}^j are Christoffel symbols of the second kind [144]. This expression involves not only the rate of change of the vector field itself, as we move along the cortical model, but also the rate of change of the local basis, which itself varies due to the intrinsic curvature of the cortex. On a surface with no intrinsic curvature, the extra terms (Christoffel symbols) vanish. The Christoffel symbols, expressed in terms of derivatives of the metric tensor components $g_{jk}(\mathbf{x})$, are calculated from the cortical model:

$$\Gamma_{jk}^i = \frac{1}{2} g^{il} \left(\partial g_{lj} / \partial x^k + \partial g_{lk} / \partial x^j - \partial g_{jk} / \partial x^l \right). \quad (A3)$$

Scalar, vector and tensor quantities, in addition to the Christoffel symbols required to implement the diffusion operators on a curved manifold are evaluated by finite differences. These correction terms are then used in the solution of the Dirichlet problem [145] for matching one cortex with another.

A variational formulation for surface mappings

A final complication is that different metric tensors $g_{jk}(\mathbf{r}_p)$ and $h_{jk}(\mathbf{r}_q)$ relate: (1) the physical domain of the input data to the computation mesh (via mapping D_p^{-1}); and (2) the solution on the computation mesh to the output data domain (via mapping D_q). To address this problem, two different approaches are possible, using either (1) simultaneous covariant regularization, or (2) a variational formulation based on Polyakov actions and Beltrami flows (concepts from high-energy physics). In the first approach (Fig. 7), the PDE $L^{\ddagger}\mathbf{u}(\mathbf{r}_q) = -\mathbf{F}$ is solved first, to find a flow field $T_q : \mathbf{r} \rightarrow \mathbf{r} - \mathbf{u}(\mathbf{r})$ on the target spherical map with anatomically driven boundary conditions $\mathbf{u}(\mathbf{r}_q) = \mathbf{u}_0(\mathbf{r}_q)$, $\forall \mathbf{r}_q \in M_0 \cup M_1$. Here $L^{\ddagger\ddagger}$ is the covariant adjustment of the differential operator L with respect to the tensor field $h_{jk}(\mathbf{r}_q)$ induced by D_q . Next, the PDE $L^{\dagger}\mathbf{u}(\mathbf{r}_p) = -\mathbf{F}$ is solved, to find a reparameterization $T_p : \mathbf{r} \rightarrow \mathbf{r} - \mathbf{u}(\mathbf{r})$ of the initial spherical map with boundary conditions $\mathbf{u}(\mathbf{r}_p) = \mathbf{0}$, $\forall \mathbf{r}_p \in M_0 \cup M_1$. Here $L^{\dagger\dagger}$ is the covariant adjustment of L with respect to the tensor field $g_{jk}(\mathbf{r}_p)$ induced by D_p . The full cortical matching field (Fig. 7, top right) is then defined as $\mathbf{x} \rightarrow D_q(F_{pq}(D_p^{-1}(\mathbf{x}))$ with $F_{pq} = (T_q)^{-1} \circ (T_p)^{-1}$.

A second (conceptually related) approach uses a variational formulation to establish a p -harmonic map from one surface to the other [23]. If P and Q are cortical surfaces with metric tensors $g_{jk}(u^i)$ and $h_{jk}(\zeta^\alpha)$ defined in local coordinates u^i and ζ^α ($i, \alpha = 1, 2$), the energy density of a map between the surfaces $\zeta(u) : (P, g) \rightarrow (Q, h)$ is the functional $e(\zeta) : P \rightarrow R$ defined in local coordinates as:

$$e(\xi)(u) = g^{ij}(u) \partial \xi^\alpha(u) / \partial u^i \partial \xi^\beta(u) / \partial u^j h_{\alpha\beta}(\xi(u)) \quad (\text{A4})$$

The Dirichlet energy of the mapping $\zeta(u)$ (i.e. the generalization of the Hilbert space norm to curved spaces) is defined as:

$$E(\xi) = \int_P e(\xi)(u) dP, \quad (\text{A5})$$

where

$$dP = \left(\sqrt{\det[g_{ij}]} \right) du^1 du^2. \quad (\text{A6})$$

The Euler equations, whose solution $\zeta^\alpha(u)$ minimizes the mapping energy, are

$$0 = L(\xi^i) = \sum_{m=1}^2 \partial / \partial u^m \left[\left(\sqrt{\det[g^{ru}]} \sum_{l=1}^2 g_{ur}^{ml} \partial \xi^i / \partial u^l \right) \right] (i=1, 2), \quad (\text{A7})$$

[146]. These equations can be discretized to produce a Beltrami flow [140] or a quasilinear elliptic system [146] whose solution is a harmonic map from one surface to the other. The major concepts of this approach are that the resulting harmonic map: (1) minimizes the change in metric from one surface to the other; and (2) is again independent of the parameterizations (spherical or planar) used for each surface.

References

- [1]. Toga, AW.; Mazziotta, JC. Brain Mapping: The Methods. Academic Press; New York: 1996.
- [2]. Toga, AW. Brain Warping. Academic Press; New York: 1998.

- [3]. Damasio, H. Human Brain Anatomy in Computerized Images. Oxford University Press; Oxford: 1995.
- [4]. Kikinis R, Shenton ME, Iosifescu DV, McCarley RW, Saiviroonporn P, Hokama HH, Robatino A, Metcalf D, Wible CG, Portas CM, Donnino R, Jolesz F. A digital brain atlas for surgical planning, model-driven segmentation, and teaching. *IEEE Transactions on Visualization and Composition Graphics* 1996;2(3):232–241.
- [5]. Talairach, J.; Szikla, G. *Atlas d'Anatomie Stereotaxique du Telencephale: Etudes Anatomo-Radiologiques*. Masson&Cie; Paris: 1967.
- [6]. Schaltenbrand, G.; Wahren, W. *Atlas for Stereotaxy of the Human Brain*. Vol. 2nd ed.. Thieme; Stuttgart: 1977.
- [7]. Talairach, J.; Tournoux, P. *Co-planar Stereotaxic Atlas of the Human Brain*. Thieme; New York: 1988.
- [8]. Ono, M.; Kubik, S.; Abernathey, CD. *Atlas of the Cerebral Sulci*. Thieme; Stuttgart: 1990.
- [9]. Duvernoy, HM. *The Human Brain*. Springer; New York: 1991.
- [10]. Brodmann, K. Some Papers on the Cerebral Cortex, translated as: On the Comparative Localization of the Cortex. Thomas; IL Springfield: 1960. *Vergleichende Lokalisationslehre der Grosshirnrinde in ihren Prinzipien dargestellt auf Grund des Zellenbaues*, Barth, Leipzig; p. 201-230.1909
- [11]. Smith GE. A new topographical survey of the human cerebral cortex, being an account of the distribution of the anatomically distinct cortical areas and their relationship to the cerebral sulci. *Journal of Anatomy* 1907;41:237–254.
- [12]. Mai, J.; Assheuer, J.; Paxinos, G. *Atlas of the Human Brain*. Academic Press; New York: 1997.
- [13]. Geyer S, Schleicher A, Zilles K. The somatosensory cortex of man: cytoarchitecture and regional distributions of receptor binding sites. *NeuroImage* 1997;6(1):27–45. [PubMed: 9245653]
- [14]. Minoshima S, Koeppe RA, Frey KA, Ishihara M, Kuhl DE. PET stereotactic atlas of the human brain: aid for visual interpretation of functional brain images. *Journal of Nuclear Medicine* 1994;35:949–954. [PubMed: 8195881]
- [15]. Le Bihan D. Functional MRI of the brain: principles, applications and limitations. *Neuroradiology* 1996;23(1):1–5.
- [16]. Avoli M, Hwa GC, Kostopoulos G, Oliver A, Villemure JG. Electrophysiological analysis of human neocortex in vitro: experimental techniques and methodological approaches. *Canadian Journal of Neurological Sciences* 1991;18:636–639. [PubMed: 1777884]
- [17]. Palovcik RA, Reid SA, Principe JC, Albuquerque A. 3D computer animation of electrophysiological responses. *Journal of Neuroscience Methods* 1992;41:1–9. [PubMed: 1578897]
- [18]. Van Essen DC, Maunsell JHR. Hierarchical organization and functional streams in the visual cortex. *Trends in Neurological Science* 1983;6:370–375.
- [19]. Berger H. Über das Elektrenkephalogramm des Menschen. *Archiv Fuer Psychiatre und Nervenkrankheiten* 1929;87:527–580.
- [20]. Penfield W, Boldrey E. Somatic motor and sensory representation in the cerebral cortex of man as studied by electrical stimulation. *Brain* 1937;60:389–443.
- [21]. Mazziotta JC, Toga AW, Evans AC, Fox P, Lancaster J. A probabilistic atlas of the human brain: theory and rationale for its development. *NeuroImage* 1995;2:89–101. [PubMed: 9343592]
- [22]. Mega MS, Chen S, Thompson PM, Woods RP, Karaca TJ, Tiwari A, Vinters H, Small GW, Toga AW. Mapping pathology to metabolism: coregistration of stained whole brain sections to PET in Alzheimer's disease. *NeuroImage* 1997;5(147153):1997.
- [23]. Thompson PM, Giedd JN, Woods RP, MacDonald D, Evans AC, Toga AW. Growth patterns in the developing human brain detected using continuum-mechanical tensor maps. *Nature* 2000;404:190–193. [PubMed: 10724172]
- [24]. Seitz RJ, Bohm C, Greitz T, Roland PE, Eriksson L, Blomqvist G, Rosenqvist G, Nordell B. Accuracy and precision of the computerized brain atlas programme for localization and quantification in positron emission tomography. *Journal of Cerebral Blood Flow and Metabolism* 1990;10:443–457. [PubMed: 2347878]

- [25]. Evans AC, Dai W, Collins DL, Neelin P, Marrett S. Warping of a computerized 3D atlas to match brain image volumes for quantitative neuroanatomical and functional analysis. SPIE Medical Imaging 1991;1445:236–247.
- [26]. Lehmann ED, Hawkes D, Hill D, Bird C, Robinson G, Colchester A, Maisley M. Computer-aided interpretation of SPECT images of the brain using an MRI-derived neuroanatomic atlas. Medical Informatics 1991;16:151–166. [PubMed: 1921560]
- [27]. Tiede U, Bomans M, Höhne KH, Pommert A, Riemer M, Schiemann T, Schubert R, Lierse W. A computerized 3D atlas of the human skull and brain. American Journal of Neuroradiology 1993;14:551–559. [PubMed: 8517340]
- [28]. Ingvar M, Eriksson L, Greitz T, Stonelander S, et al. Methodological aspects of brain activation studies — cerebral blood flow determined with $[O-15]$ -butanol and positron emission tomography. Journal of Cerebral Blood Flow and Metabolism 1994;14(4):628–638. [PubMed: 8014210]
- [29]. Fox PT, Perlmutter JS, Raichle M. A stereotactic method of localization for positron emission tomography. Journal of Computer Assisted Tomography 1985;9(1):141–153. [PubMed: 3881487]
- [30]. Fox PT, Mintun MA, Reiman EM, Raichle ME. Enhanced detection of focal brain responses using inter-subject averaging and change distribution analysis of subtracted PET images. Journal of Cerebral Blood Flow and Metabolism 1988;8:642–653. [PubMed: 3262113]
- [31]. Friston KJ, Passingham RE, Nutt JG, Heather JD, Sawle GV, Frackowiak RSJ. Localization in PET images: direct fitting of the intercommissural (AC-PC) line. Journal of Cerebral Blood Flow and Metabolism 1989;9:690–695. [PubMed: 2789231]
- [32]. Friston KJ, Frith CD, Liddle PF, Frackowiak RSJ. Plastic transformation of PET images. Journal of Computer Assisted Tomography 1991;9(1):141–153.
- [33]. Roland PE, Zilles K. Brain atlases — a new research tool. Trends in Neurosciences 1994;17(11):458–467. [PubMed: 7531886]
- [34]. Evans, AC.; Collins, DL.; Milner, B. An MRI-based stereotactic brain atlas from 300 young normal subjects; Proceedings of the 22nd Symposium of the Society for Neuroscience; Anaheim. 1992; p. 408
- [35]. Evans, AC.; Collins, DL.; Neelin, P.; MacDonald, D.; Kamber, M.; Marrett, TS. Three-dimensional correlative imaging: applications in human brain mapping. In: Thatcher, RW.; Hallett, M.; Zeffiro, T.; John, ER.; Huerta, M., editors. Functional Neuroimaging: Technical Foundations. 1994. p. 145–162.
- [36]. West J, Fitzpatrick JM, Wang MY, Dawant BM, Maurer CR, Kessler RM, Maciunas RJ, Barillot C, Lemoine D, Collignon A, Maes F, Suetens P, Vandermeulen D, van den Elsen PA, Napel S, Sumanaweera TS, Harkness B, Hemler BF, Hill DLG, Hawkes DL, Studholme C, Maintz JBA, Viergever MA, Malandain G, Pennec X, Noz ME, Maguire GQ, Pollack M, Pelizzari CA, Robb RA, Hanson R, Woods RP. Comparison and evaluation of retrospective intermodality brain image registration techniques. Journal of Computer Assisted Tomography 1997;21(554566)
- [37]. Maintz JBA, Viergever MA. A survey of medical image registration. Medical Image Analysis 1998;2(1):1–36. [PubMed: 10638851]
- [38]. Collins DL, Neelin P, Peters TM, Evans AC. Automatic 3D Intersubject registration of MR volumetric data into standardized Talairach space. Journal of Computer Assisted Tomography 1994;18(2):192–205. [PubMed: 8126267]
- [39]. Collins DL, Peters TM, Evans AC. An automated 3D non-linear image deformation procedure for determination of gross morphometric variability in the human brain. Proceedings of the Visualization in Biomedical Compositions (SPIE) 1994;3:180–190.
- [40]. Collins DL, Holmes CJ, Peters TM, Evans AC. Automatic 3D model-based neuroanatomical segmentation. Human Brain Mapping 1995;3:190–208.
- [41]. Woods RP, Cherry SR, Mazziotta JC. Rapid automated algorithm for aligning and reslicing PET images. Journal of Computer Assisted Tomography 1992;16:620–633. [PubMed: 1629424]
- [42]. Viola, PA.; Wells, WM. Alignment by maximization of mutual information; Fifth IEEE International Conference on Computer Vision; Cambridge, MA. 1995; p. 16-23.
- [43]. Collignon, A.; Maes, F.; Delaere, D.; Vandermeulen, D.; Suetens, P.; Marchal, G. Automated multi-modality image registration based on information theory. In: Bizais, Y.; Barillot, C.; DiPaola, R., editors. Information Processing in Medical Imaging. Kluwer; Dordrecht: 1995. p. 263–274.

- [44]. Wells WM, Viola P, Atsumi H, Nakajima S, Kikinis R. Multimodal volume registration by maximization of mutual information. *Medical Image Analysis* 1997;1(1):35–51. [PubMed: 9873920]
- [45]. Kim B, Boes JL, Frey KA, Meyer CR. Mutual information for automated unwarping of rat brain autoradiographs. *Neuroimage* 1997;5(1):31–40. [PubMed: 9038282]
- [46]. Woods RP, Mazziotta JC, Cherry SR. MRI-PET registration with automated algorithm. *Journal of Computer Assisted Tomography* 1993;17:536–546. [PubMed: 8331222]
- [47]. Missir O, Dutheil-Desclercs C, Meder JF, Musolino A, Fredy D. Central sulcus patterns at MRI. *Journal of Neuroradiology* 1989;16:133–144.
- [48]. Rademacher J, Caviness VS Jr, Steinmetz H, Galaburda AM. Topographical variation of the human primary cortices: implications for neuroimaging, brain mapping and neurobiology. *Cerebral Cortex* 1993;3(4):313–329. [PubMed: 8400809]
- [49]. Stensaas SS, Eddington DK, Dobelle WH. The topography and variability of the primary visual cortex in man. *Journal of Neurosurgery* 1974;40:747–755. [PubMed: 4826600]
- [50]. Rajkowska G, Goldman-Rakic P. Cytoarchitectonic definition of pre-frontal areas in the normal human cortex: II. Variability in locations of areas 9 and 46 and relationship to the talairach coordinate system. *Cerebral Cortex* 1995;5(4):323–337. [PubMed: 7580125]
- [51]. Geschwind N, Levitsky W. Human brain: left-right asymmetries in temporal speech region. *Science* 1968;161:186. [PubMed: 5657070]
- [52]. Steinmetz H, Furst G, Freund H-J. Cerebral cortical localization: application and validation of the proportional grid system in MR imaging. *Journal of Computer Assisted Tomography* 1989;13(1): 10–19. [PubMed: 2642922]
- [53]. Steinmetz H, Furst G, Freund H-J. Variation of perisylvian and calcarine anatomic landmarks within stereotaxic proportional coordinates. *American Journal of Neuroradiology* 1990;11(6):1123–1130. [PubMed: 2124038]
- [54]. Thompson PM, Schwartz C, Toga AW. High-resolution random mesh algorithms for creating a probabilistic 3D surface atlas of the human brain. *NeuroImage* 1996;3:19–34. [PubMed: 9345472]
- [55]. Thompson PM, Schwartz C, Lin RT, Khan AA, Toga AW. 3D statistical analysis of sulcal variability in the human brain. *Journal of Neuroscience* 1996;16(13):4261–4274. [PubMed: 8753887]
- [56]. Thompson, PM.; Mega, MS.; Woods, RP.; Blanton, RE.; Moussai, J.; Zoumalan, CI.; Aron, J.; Cummings, JL.; Toga, AW. A probabilistic atlas of the human brain in Alzheimer's disease: emerging patterns of variability, asymmetry and degeneration; Fifth International Conference on Functional Mapping of the Human Brain; Dusseldorf, Germany. June 1999;
- [57]. Meltzer, CC.; Frost, JJ. Partial volume correction in emission-computed tomography: focus on Alzheimer disease. In: Thatcher, RW.; Hallett, M.; Zeffiro, T.; John, ER.; Huerta, M., editors. *Functional Neuroimaging: Technical Foundations*. Academic Press; New York: 1994. p. 163–170.
- [58]. Woods RP. Modeling for intergroup comparisons of imaging data. *NeuroImage* 1996;4(3):84–94.
- [59]. Watson JDG, Myers R, Frackowiak RSJ, Hajnal JV, Woods RP, Mazziotta JC, Shipp S, Zeki S. Area V5 of the human brain: evidence from a combined study using positron emission tomography and magnetic resonance imaging. *Cerebral Cortex* 1993;3:79–94. [PubMed: 8490322]
- [60]. Broit, C. PhD Dissertation. USA University of Pennsylvania; 1981. Optimal registration of deformed images.
- [61]. Bajcsy R, Kovacic S. Multiresolution elastic matching. *Computer Vision, Graphics and Image Processing* 1989;46:1–21.
- [62]. Gee JC, Reivich M, Bajcsy R. Elastically deforming an atlas to match anatomical brain images. *Journal of Computer Assisted Tomography* 1993;17(2):225–236. [PubMed: 8454749]
- [63]. Gee JC, LeBriquer L, Barillot C, Haynor DR, Bajcsy R, Institute for Research in Cognition Science. Bayesian approach to the brain image matching problem. April;1995 Technical Report 95-08
- [64]. Thurfjell L, Bohm C, Greitz T, Eriksson L. Transformations and algorithms in a computerized brain atlas. *IEEE Transactions on Nuclear Science (part 1)* 1993;40(4):1167–1191.
- [65]. Christensen, GE.; Rabbitt, RD.; Miller, MI. A deformable neuroanatomy textbook based on viscous fluid mechanics; 27th Annual Conference on Information Sciences and Systems; 1993; p. 211–216.

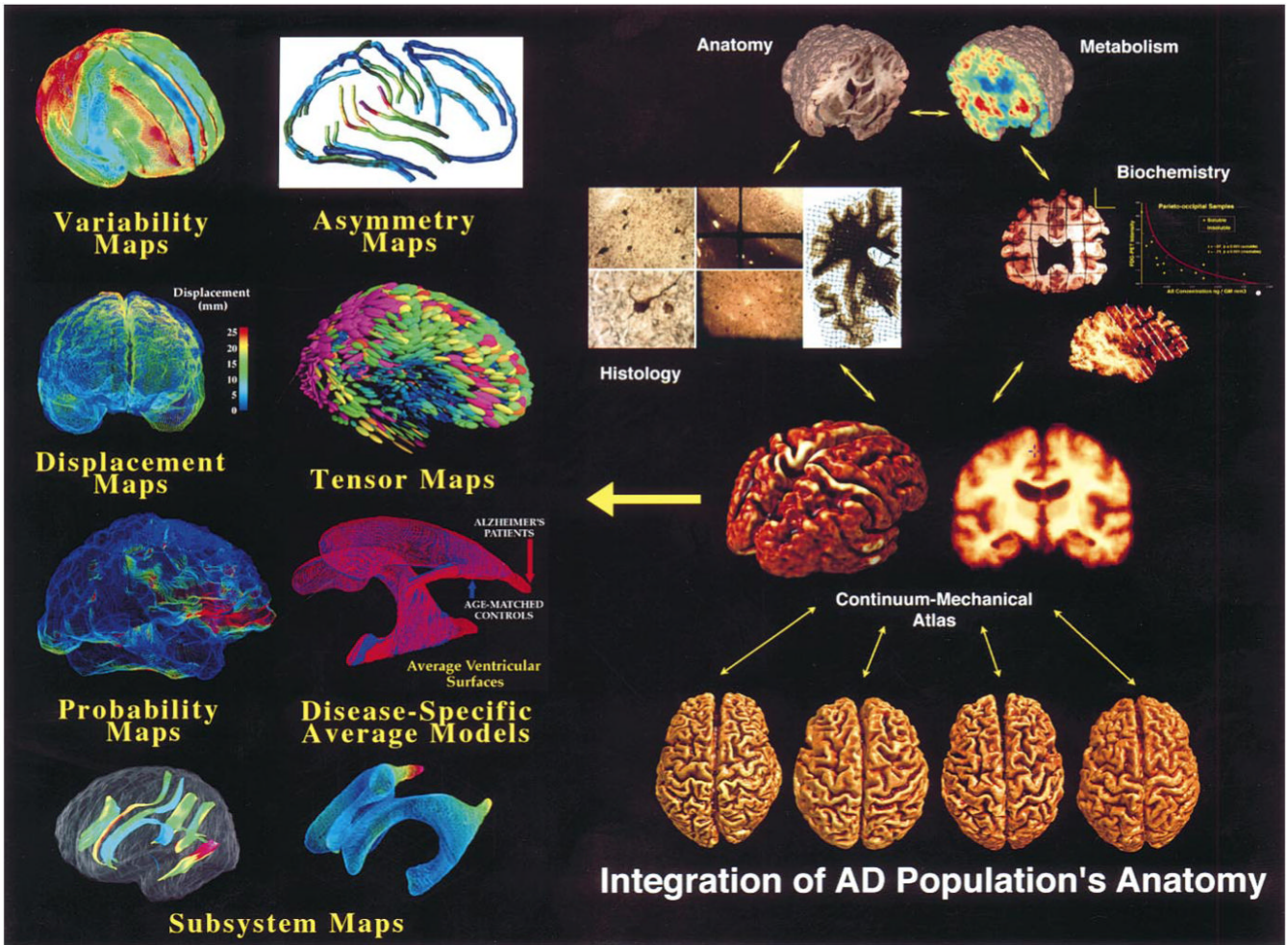
- [66]. Christensen GE, Rabbitt RD, Miller MI. Deformable templates using large deformation kinematics. *IEEE Transactions on Image Processing* 1996;5(10):1435–1447. [PubMed: 18290061]
- [67]. Thirion, J-P. INRIA Projet Epidaure; France: 1995. Fast non-rigid matching of medical images. INRIA Internal Report 2547
- [68]. Rabbitt RD, Weiss JA, Christensen GE, Miller MI. Mapping of hyperelastic deformable templates using the finite element method. *Proceedings of the SPIE* 1995;2573:252–265.
- [69]. Davatzikos C. Spatial normalization of 3D brain images using deformable models. *Journal of Computer Assisted Tomography* 1996;20(4):656–665. [PubMed: 8708076]
- [70]. Thompson PM, Toga AW. A surface-based technique for warping 3-dimensional images of the brain. *IEEE Transactions on Medical Imaging* 1996;15(4):1–16.
- [71]. Bro-Nielsen, M.; Gramkow, C. Fast fluid registration of medical images. In: Höhne, KH.; Kikinis, R., editors. *Visualization in Biomedical Computing*, Hamburg, Germany, Lecture Notes in Computer Science. Vol. 1131. Springer; Berlin: 1996. p. 267–276.
- [72]. Schormann T, Henn S, Zilles K. A new approach to fast elastic alignment with applications to human brains. *Proceedings of the Visualization in Biomedical Computation* 1996;4:337–342.
- [73]. Ashburner J, Neelin P, Collins DL, Evans AC, Friston KJ. Incorporating prior knowledge into image registration. *Neuroimage* 1997;6(4):344–352. [PubMed: 9417976]
- [74]. Woods RP, Grafton ST, Watson JDG, Sicotte NL, Mazziotta JC. Automated image registration: II. Intersubject validation of linear and nonlinear models. *Journal of Computer Assisted Tomography* 1998;22in press
- [75]. Gabrani M, Tretiak OJ. Surface-based matching using elastic transformations. *Pattern Recognition* 1999;32(1):87–97.
- [76]. Kjems U, Strother SC, Anderson J, Law I, Hansen LK. Enhancing the multivariate signal of [¹⁵O]-water PET studies with a new nonlinear neuroanatomical registration algorithm. *IEEE Transactions on Medical Imaging* 1999;18(4):306–319. [PubMed: 10385288]
- [77]. Lester, H.; Arridge, SR.; Jansons, KM.; Lemieux, L.; Hajnal, JV.; Oatridge, A. Non-linear registration with the variable viscosity fluid algorithm. IPMI'99; 16th International Conference on Information Processing in Medical Imaging; 2000; in press
- [78]. Miller MI, Christensen GE, Amit Y, Grenander U. Mathematical textbook of deformable neuroanatomies. *Proceedings of the National Academy of Sciences USA* 1993;90:11944–11948.
- [79]. Sandor SR, Leahy RM. Matching deformable atlas models to pre-processed magnetic resonance brain images. *Proceedings of the IEEE Conference on Image Processing* 1994;3:686–690.
- [80]. Sandor, SR.; Leahy, RM. Towards automated labeling of the cerebral cortex using a deformable atlas. In: Bizais, Y.; Barillot, C.; Di Paola, R., editors. *Information Processing in Medical Imaging*. Jun. 1995 p. 127–138.
- [81]. Rizzo G, Gilardi MC, Prinster A, Grassi F, Scotti G, Cerutti S, Fazio F. An elastic computerized brain atlas for the analysis of clinical PET/SPET data. *European Journal of Nuclear Medicine* 1995;22(11):1313–1318. [PubMed: 8575483]
- [82]. Friston KJ, Holmes AP, Worsley KJ, Poline JP, Frith CD, Frackowiak RSJ. Statistical parametric maps in functional imaging: a general linear approach. *Human Brain Mapping* 1995;2:189–210.
- [83]. Thompson, PM.; Toga, AW. Anatomically-driven strategies for high-dimensional brain image registration and pathology detection. In: Toga, AW., editor. *Brain Warping*. Academic Press; New York: Nov. 1998 p. 311–336.
- [84]. Christensen, GE.; Rabbitt, RD.; Miller, MI.; Joshi, SC.; Grenander, U.; Coogan, TA.; Van Essen, DC. Topological properties of smooth anatomic maps. In: Bizais, Y.; Barillot, C.; Di Paola, R., editors. *Information Processing in Medical Imaging*. Jun. 1995 p. 101–112.
- [85]. Dupuis P, Grenander U, Miller MI. Variational problems on flows of diffeomorphisms for image matching. *Quarterly of Applied Mathematics* 1998;56(3):587–600.
- [86]. Davatzikos C, Vaillant M, Resnick SM, Prince JL, Letovsky S, Bryan RN. A computerized approach for morphological analysis of the corpus callosum. *Journal of Computer Assisted Tomography* 1996;20(1):88–97. [PubMed: 8576488]
- [87]. Collins, DL.; Le Goualher, G.; Venugopal, R.; Caramanos, A.; Evans, AC.; Barillot, C. Cortical constraints for non-linear cortical registration. In: Höhne, KH.; Kikinis, R., editors. *Visualization*

- in Biomedical Computing, Hamburg, Germany, Lecture Notes in Computer Science. Vol. 1131. Springer; Berlin: 1996. p. 307-316.
- [88]. Toga, AW. Visualization and warping of multimodality brain imagery. In: Thatcher, RW.; Hallett, M.; Zeffiro, T.; John, ER.; Huerta, M., editors. Functional Neuroimaging: Technical Foundations. 1994. p. 171-180.
- [89]. Toga AW, Ambach K, Quinn B, Hutchin M, Burton JS. Postmortem anatomy from cryosectioned whole human brain. *Journal of Neuroscience Methods* 1994;54(2):239–252. [PubMed: 7869755]
- [90]. Toga, AW.; Thompson, PM. Measuring, mapping, and modeling brain structure and function. SPIE Lecture Notes; SPIE Medical Imaging Symposium; CA Newport Beach, USA. February 1997; 1997. in press
- [91]. Haller JW, Banerjee A, Christensen GE, Gado M, Joshi S, Miller MI, Sheline Y, Vannier MW, Csernansky JG. Three-dimensional hippocampal M.R., morphometry with high-dimensional transformation of a neuroanatomic atlas. *Radiology* 1997;202(2):504–510. [PubMed: 9015081]
- [92]. Iosifescu DV, Shenton ME, Warfield SK, Kikinis R, Dengler J, Jolesz FA, McCarley RW. An automated registration algorithm for measuring MRI subcortical brain structures. *NeuroImage* 1997;6(1):13–25. [PubMed: 9245652]
- [93]. Thompson PM, MacDonald D, Mega MS, Holmes CJ, Evans AC, Toga AW. Detection and mapping of abnormal brain structure with a probabilistic atlas of cortical surfaces. *Journal of Computer Assisted Tomography* 1997;21(4):567–581. [PubMed: 9216760]
- [94]. Thompson PM, Moussai J, Khan AA, Zohoori S, Goldkorn A, Mega MS, Small GW, Cummings JL, Toga AW. Cortical variability and asymmetry in normal aging and Alzheimer's disease. *Cerebral Cortex* 1998;8(6):492–509. [PubMed: 9758213]
- [95]. Warfield S, Dengler J, Zaers J, Guttmann CRG, Wells WM, Ettinger GJ, Hiller J, Kikinis R. Automatic identification of gray matter structures form MRI to improve the segmentation of white matter lesions. Proceedings of the Medical Robotics & Computer Assisted Surgery (MRCAS) November 4-7;1995 :55–62.
- [96]. Bookstein F. Principal warps: thin-plate splines and the decomposition of deformations. *IEEE Transactions on Pattern Analysis and Machine Intelligence* 1989;11(6):567–585.
- [97]. Bookstein FL. Landmark methods for forms without landmarks: morphometrics of group differences in outline shape. *Medical Image Analysis* 1997;1(3):225–243. [PubMed: 9873908]
- [98]. Subsol G, Roberts N, Doran M, Thirion JP, Whitehouse GH. Automatic analysis of cerebral atrophy. *Magnetic Resonance and Imaging* 1997;15(8):917–927.
- [99]. Thompson PM, Toga AW. Detection, visualization and animation of abnormal anatomic structure with a deformable probabilistic brain atlas based on random vector field transformations. *Medical Image Analysis* 1997;1(4):271–294. [PubMed: 9873911]paper, with video sequences on CD-ROM with Journal Issue, November 1997
- [100]. Grenander, U.; Miller, MI. Technical Report. Department of Mathematics, Brown University; 1998. Computational anatomy: an emerging discipline.
- [101]. Toga, AW.; Thompson, PM.; Payne, BA. Modeling morphometric changes of the brain during development. In: Thatcher, RW.; Lyon, GR.; Rumsey, J.; Krasnegor, N., editors. Chapter in: *Developmental Neuroimaging: Mapping the Development of Brain and Behavior*. Academic Press; New York: 1996.
- [102]. Andreasen NC, Arndt S, Swayze V, Cizadlo T, Flaum M, O'Leary D, Ehrhardt JC, Yuh WTC. Thalamic abnormalities in schizophrenia visualized through magnetic resonance image averaging. *Science* October;1994 266:294–298. [PubMed: 7939669]
- [103]. Ge Y, Fitzpatrick JM, Kessler RM, Jeske-Janicka M. Intersubject brain image registration using both cortical and subcortical landmarks. *SPIE Image Processing* 1995;2434:81–95.
- [104]. Thompson PM, Woods RP, Mega MS, Toga AW. Mathematical/computational challenges in creating deformable and probabilistic atlases of the brain. *Human Brain Mapping* 2000;9(2):81–92. [PubMed: 10680765]
- [105]. Thompson, PM.; Mega, MS.; Toga, AW. Disease-specific brain atlases. In: Toga, AW.; Mazziotta, JC., editors. Book Chapter in: *Brain Mapping: The Disorders*. Academic Press; New York: 2000.

- [106]. Thompson, PM.; Mega, MS.; Narr, KL.; Sowell, ER.; Blanton, RE.; Toga, AW. Brain image analysis and atlas construction. In: Fitzpatrick, M., editor. SPIE Handbook on Medical Image Analysis. Society of Photo-Optical Instrumentation Engineers (SPIE) Press; 2000.
- [107]. Thompson, PM.; Narr, KL.; Blanton, RE.; Toga, AW. Mapping structural alterations of the corpus callosum during brain development and degeneration. In: Iacoboni, M.; Zaidel, E., editors. The Corpus Callosum. MIT Press; Cambridge, MA: 2000. in press
- [108]. Otaky N, Paus T, D'Avirro D, Gutmans D, MacDonald D, Caramanos Z, Tomaioiu F, Evans AC. Volumetric analysis of the human cingulate, paracingulate, and superior rostral sulci. Society for Neuroscience Abstracts 1995;21(1):154.
- [109]. Paus T, Tomaioiu F, Otaky N, MacDonald D, Petrides M, Atlas J, Morris R, Evans AC. Human cingulate and paracingulate sulci: pattern, variability, asymmetry and probabilistic map. *Cerebral Cortex* 1996;6:207–214. [PubMed: 8670651]
- [110]. Zijdenbos AP, Dawant BM. Brain segmentation and white matter lesion detection in MR images. *Critical Reviews on Biomedical Engineering* 1994;22(56):401–465.
- [111]. Mega MS, Dinov ID, Lee L, Woods RP, Thompson PM, Holmes CJ, Back CL, Collins DL, Evans AC, Toga AW. Dissecting neural networks underlying the retrieval deficit from the amnestic memory disorder using [99m Tc]-HMPAO-SPECT. *Proceedings of the American Behavioral Neurological Society*. February;1998
- [112]. Dinov ID, Thompson PM, Woods RP, Mega MS, Holmes CJ, Sumners D, Saxena S, Toga AW. Probabilistic sub-volume partitioning techniques for determining the statistically significant regions of activation in stereotaxic functional data. *Journal of Computer Assisted Tomography* 2000;24(1): 128–138. [PubMed: 10667672]
- [113]. Sowell ER, Thompson PM, Holmes CJ, Jernigan TL, Toga AW. Progression of structural changes in the human brain during the first three decades of life: in vivo evidence for post-adolescent frontal and striatal maturation. *Nature Neuroscience*. 1999
- [114]. Carman GJ, Drury HA, Van Essen DC. Computational methods for reconstructing and unfolding the cerebral cortex. *Cerebral Cortex* 1995;5(6):506–517. [PubMed: 8590824]
- [115]. Schwartz EL, Merker B. Computer-aided neuroanatomy: differential geometry of cortical surfaces and an optimal flattening algorithm. *IEEE Computer Graphics and Applications* 1986;6:36–44.
- [116]. Drury, HA.; Van Essen, DC.; Joshi, SC.; Miller, MI. Analysis and comparison of areal partitioning schemes using two-dimensional fluid deformations, poster presentation. NeuroImage; Second International Conference on Functional Mapping of the Human Brain; USA MA Boston. June 17-21; 1996. p. S130
- [117]. Drury HA, Van Essen DC. Analysis of functional specialization in human cerebral cortex using the visible man surface based atlas. *Human Brain Mapping* 1997;5:233–237. [PubMed: 11542497]
- [118]. Dale AM, Sereno MI. Improved localization of critical activity by combining EEG and MEG with MRI cortical surface reconstruction — a linear approach 1993;5(2):162–176.
- [119]. Sereno, MI.; Dale, AM.; Liu, A.; Tootell, RBH. A surface-based coordinate system for a canonical cortex. *Neuroimage; Proceedings of the Second International Conference on Human Brain Mapping*; MA Boston. 1996; p. S252
- [120]. Fischl B, Sereno MI, Tootell RBH, Dale AM. High-resolution inter-subject averaging and a coordinate system for the cortical surface. 2000in press
- [121]. Leonard, CM. Structural variation in the developing and mature cerebral cortex: noise or signal?. In: Thatcher, RW.; Reid Lyon, G.; Rumsey, J.; Krasnegor, N., editors. *Developmental Neuroimaging: Mapping the Development of Brain and Behavior*. Academic Press; New York: 1996. p. 207-231.
- [122]. MacDonald, D.; Avis, D.; Evans, AC. Automatic parameterization of human cortical surfaces. *IPMI; Annual Symposium on Information Processing in Medical Imaging*; 1993;
- [123]. Bakircioglu M, Joshi SC, Miller MI. Landmark matching on brain surfaces via large deformation diffeomorphisms on the sphere. *Proceedings of the SPIE Medical Imaging*. 1999
- [124]. Kennedy DN, Lange N, Makris N, Bates J, Meyer J, Caviness VS Jr. Gyri of the human neocortex: an MRI-based analysis of volume and variance. *Cerebral Cortex* 1998;8(4):372–384. [PubMed: 9651132]

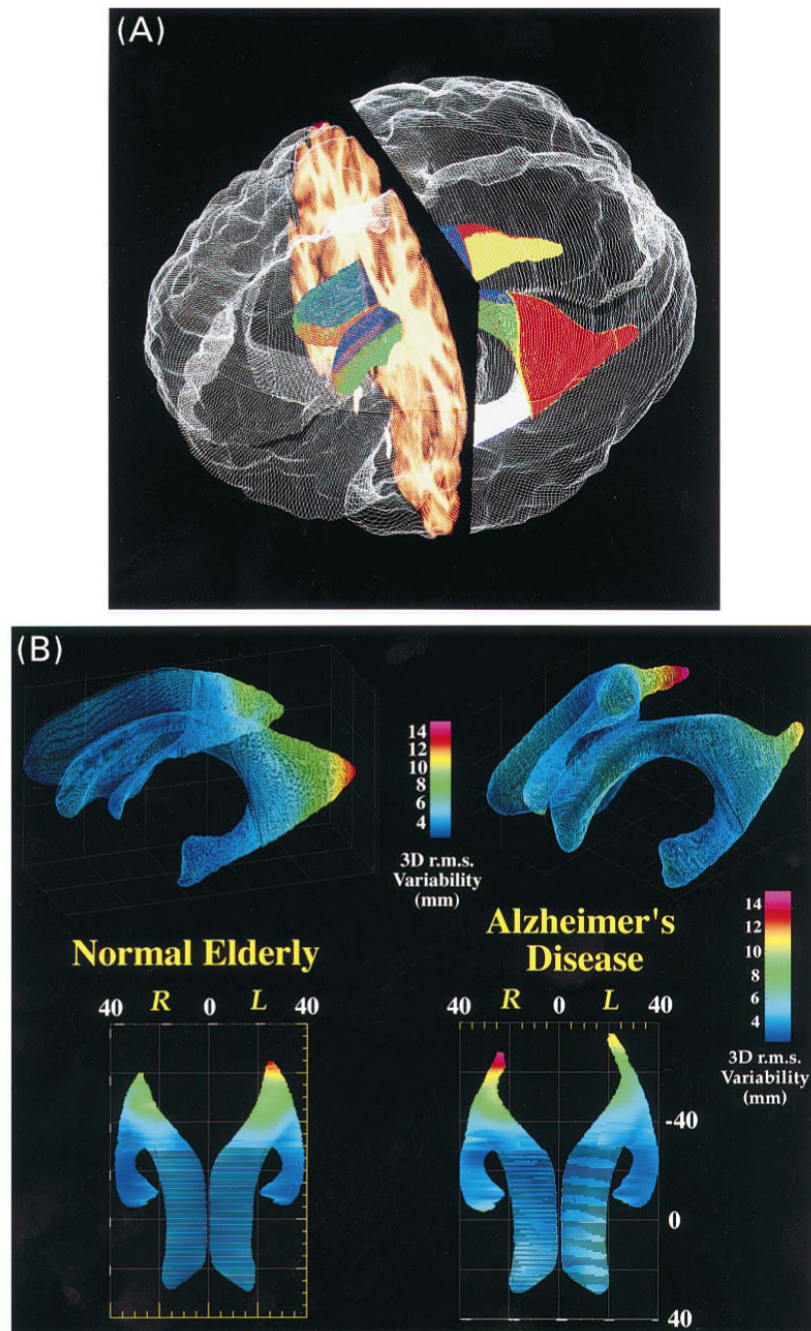
- [125]. Royackkers, N.; Desvignes, M.; Revenu, M. Construction automatique d'un atlas adaptatif des sillons corticaux. Clermont-Ferrand; 1996. p. 187-192. ORASIS 96
- [126]. Pitiot A, Thompson PM, Toga AW. Spatially and temporally adaptive elastic template matching. *IEEE Transactions on Pattern Analysis and Machine Intelligence*. 2000;in press
- [127]. Narr KL, Thompson PM, Sharma T, Moussai J, Cannestra AF, Toga AW. Mapping corpus callosum morphology in schizophrenia. *Cerebral Cortex*. 2000;in press
- [128]. Cao J, Worsley KJ. The geometry of the Hotelling's T-squared random field with applications to the detection of shape changes. *Annals of Statistics*. 2000;in press
- [129]. Ashburner J, Hutton C, Frackowiak R, Johnsrude I, Price C, Friston K. Identifying global anatomical differences: deformationbased morphometry. *Human Brain Mapping* 1998;6(56):348–357. [PubMed: 9788071]
- [130]. Gaser, C.; Kiebel, S.; Riehemann, S.; Volz, H-P.; Sauer, H. Statistical parametric mapping of structural changes in brain — application to schizophrenia research; Fourth International Conference on Functional Mapping of the Human Brain; Montreal. 1998; Poster#0718
- [131]. Le Goualher G, Procyk E, Collins DL, Venugopal R, Barillot C, Evans AC. Automated extraction and variability analysis of sulcal neuroanatomy. *IEEE Transactions on Medical Imaging* 1999;18(3):206–217. [PubMed: 10363699]
- [132]. Zoumalan, CI.; Mega, MS.; Thompson, PM.; Fuh, JL.; Lindshield, C.; Toga, AW. Mapping 3D patterns of cortical variability in normal aging and Alzheimer's disease; Annual Conference of the American Academy of Neurology; 1999;
- [133]. Amit Y, Grenander U, Piccioni M. Structural image restoration through deformable templates. *Journal of American Statistical Association* 1991;86(414):376–386.
- [134]. Joshi SC, Miller MI, Grenander U. On the geometry and shape of brain sub-manifolds. *International Journal of Pattern Recognition and Artificial Intelligence*. 1998
- [135]. Vaillant, M.; Davatzikos, C. Hierarchical matching of cortical features for deformable brain image registration; Proceedings of the Information Processing in Medical Imaging; Budapest. June 1999;
- [136]. England, MA. Year Book Medical. 1990. Colour Atlas of Life Before Birth: Normal Fetal Development.
- [137]. Fuh, JL.; Mega, MS.; Thompson, PM.; Cummings, JL.; Toga, AW. Cortical complexity maps and cognition in Alzheimer's disease; Proceedings of the 122nd Annual Meeting of the American Neurological Association; 1997;
- [138]. Gee, JC.; Bajscy, RK. Elastic matching: continuum-mechanical and probabilistic analysis. In: Toga, AW., editor. *Brain Warping*. Academic Press; San Diego: 1998.
- [139]. Mangin J-F, Frouin V, Bloch I, Regis J, Lopez-Krahe J. Automatic construction of an attributed relational graph representing the cortex topography using homotopic transformations. *SPIE* 1994;2299:110–121.
- [140]. Sochen N, Kimmel R, Malladi R. A general framework for low level vision. *IEEE Transactions on Image Processing* 1998;7(3):310–318. [PubMed: 18276251]
- [141]. Thirion, J-P.; Calmon, G. Deformation analysis to detect and quantify active lesions in 3D medical image sequences. Projet Epidaure; INRIA, France: Feb. 1997 INRIA Internal Report 3101
- [142]. Thompson, PM.; Toga, AW. Elastic image registration and pathology detection. In: Bankman, I.; Rangayyan, R.; Evans, AC.; Woods, RP.; Fishman, E.; Huang, HK., editors. Book Chapter in: *Handbook of Medical Image Processing*. Academic Press; New York: 2000. in press
- [143]. Cohen, LD.; Cohen, I. Deformable models for 3D medical images using finite elements & balloons; Proceedings: 1992 IEEE Computer Society Conference on Computer Vision and Pattern Recognition; IEEE Computer Society Press, Los Alamitos, CA. 1992; p. 592-598. Cat. No. 92 CH3168-2
- [144]. Einstein A. Covariance properties of the field equations of the theory of gravitation based on the generalized theory of relativity, 29 May 1914, published as *Kovarianzeigenschaften der Feldgleichungen der auf die verallgemeinerte Relativitätstheorie gegründeten Gravitationstheorie*. *Zeitschrift für Mathematik und Physik* 1914;63:215–225.
- [145]. Joshi, SC.; Miller, MI.; Christensen, GE.; Banerjee, A.; Coogan, TA.; Grenander, U. Hierarchical brain mapping via a generalized dirichlet solution for mapping brain manifolds, vision geometry

- IV; Proceedings of the SPIE Conference on Optical Science, Engineering and Instrumentation; CA San Diego. August 1995; 1995. p. 278-289.
- [146]. Liseikin VD. On a variational method for generating adaptive grids on N-dimensional surfaces. Doklady Akademii Nauk, CCCP 1991;319(3):546–549.

**Fig. 1.**

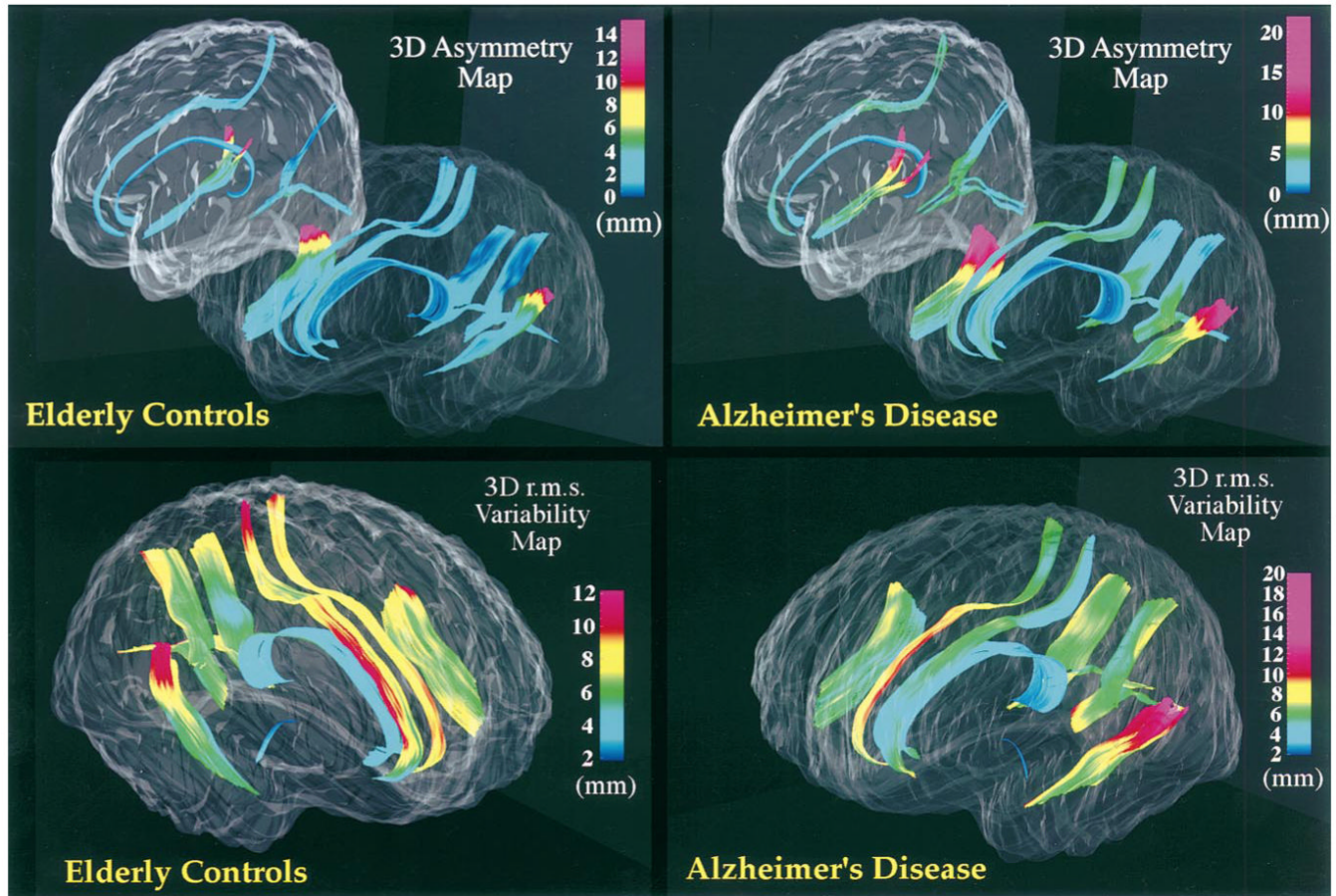
Population-based digital brain atlases. Multimodality brain atlases combine registered image data from multiple imaging devices and multiple subjects in a common coordinate space, providing a more comprehensive description of brain structure and function than can be obtained with a single modality. This schematic shows the types of maps and models contained in a disease-specific brain atlas [23], that represents the anatomy and physiology of a population of patients with Alzheimer's disease. To construct the atlas, databases of structural imaging data are used to develop detailed models of cortical structure and anatomic subsystems. These models are statistically combined to create group average models (left panels) that can be compared with a normal database. Patterns of variability, asymmetry, and disease-specific differences are also computed from the anatomic data. Specialized techniques create a well-resolved average image template for the patient population (Continuum-Mechanical Template, center right). This template provides a coordinate framework to link *in vivo* metabolic and functional data with fine-scale anatomy and biochemistry (upper right). In recent studies [22], histologic maps of post mortem neurofibrillary tangle (NFT) staining density were correlated with *in vivo* metabolism. 3D FDG-PET data, obtained 8 h before death, was compared with whole-brain cryosections acquired immediately post mortem and stained for NFTs by the Gallyas method. Using the algorithm of [70] (warped image), distorted tissue sections were elastically warped back to their configuration in the cryosection blockface (top row). A further 3D registration projected the data into premortem MR and co-registered PET

data (top right). Technical information on disease-specific atlas systems for Alzheimer's disease, schizophrenia, and a variety of pediatric disorders can be found in [23].

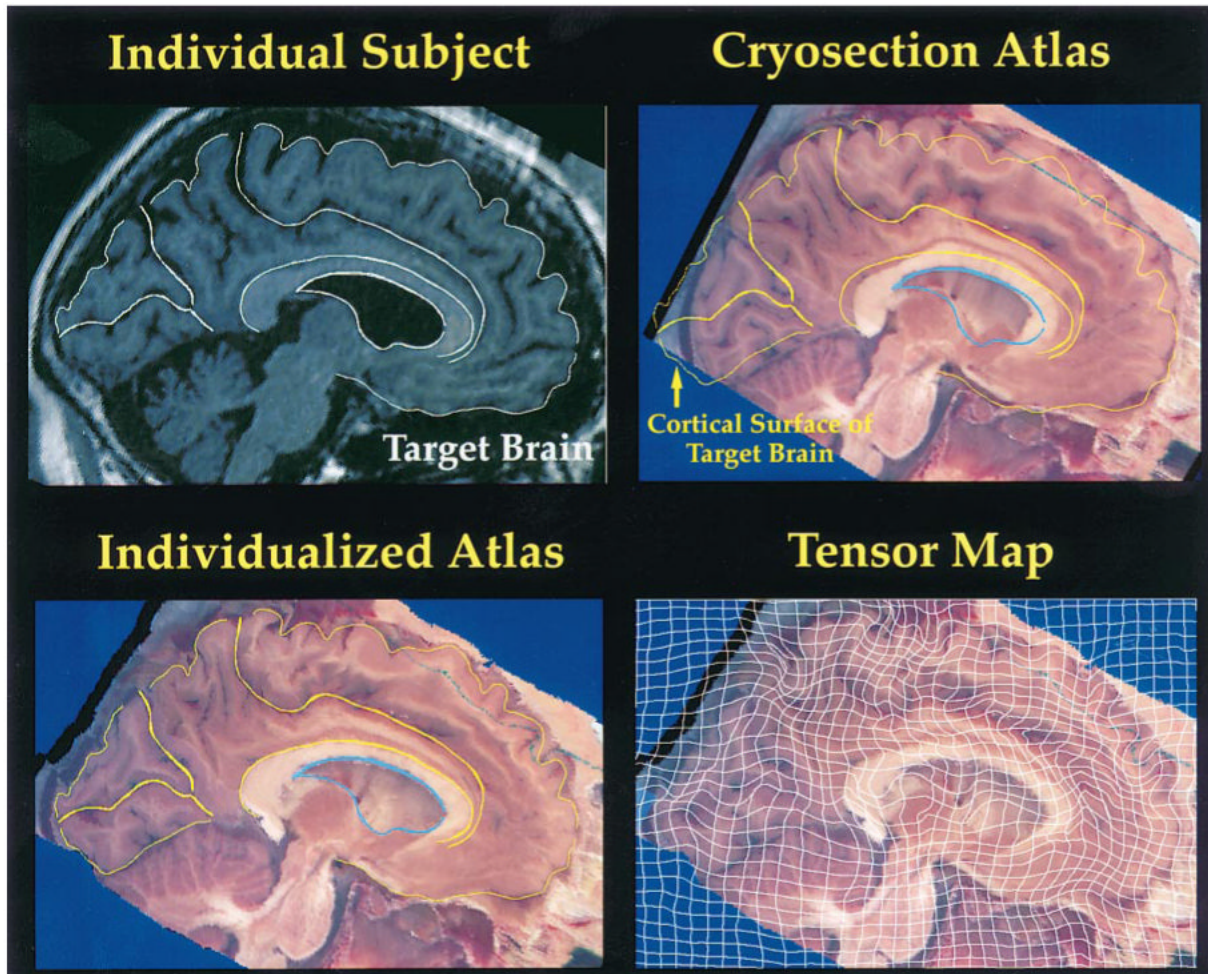
**Fig. 2.**

Population-based maps of ventricular anatomy in normal aging and Alzheimer's disease. (A). 3D parametric surface meshes [55] were used to model a connected system of 14 tissue elements at the ventricular surface (partitioned along cytoarchitectural boundaries), based on high-resolution 3D MRI scans of 10 Alzheimer's patients (age: 71.9 ± 10.9 y) and 10 controls matched for age (72.9 ± 5.6 y), gender and handedness [94]. 3D meshes representing each surface element were averaged by hemisphere in each group. (B) and (C) The color map encodes a 3D r.m.s. measure of group anatomic variability shown pointwise on an average surface representation for each group, in the Talairach stereotaxic space. Oblique side views reveal enlarged occipital horns in the Alzheimer's patients, and high stereotaxic variability in

both groups. (lower panels): A top view of these averaged surface meshes reveals localized patterns of asymmetry, variability, and displacement within and between groups. Asymmetry patterns at the ventricles and Sylvian fissure (q.v., Fig. 3) emerge only after averaging of anatomical maps in large groups of subjects. Patterns of 3D variation can be encoded probabilistically to detect structural anomalies in individual patients or groups [23,83,93,94].

**Fig. 3.**

Population-based maps of 3D structural variation and asymmetry. Statistics of 3D deformation maps can be computed to determine confidence limits on normal anatomic variation. 3D maps of anatomic variability and asymmetry are shown for 10 subjects with Alzheimer's disease (AD; age: 71.9 ± 10.9 y, and 10 normal elderly subjects matched for age (72.9 ± 5.6 y), gender, handedness and educational level [94]. Normal Sylvian fissure asymmetries (right higher) than left; $p < 0.0005$), mapped for the first time in 3D, were significantly greater in AD than in controls ($p < 0.0002$; top panels). In the 3D variability maps derived for each group (lower panels), the color encodes the root mean square magnitude of the displacement vectors required to map the surfaces from each of the ten patients' brains onto the average. Confidence limits on 3D cortical variation (lower right panel), exhibited severe increases in AD from 2-4 mm at the corpus callosum to a peak standard deviation of 19.6 mm at the posterior left Sylvian fissure.

**Fig. 4.**

A Deformable brain atlas measures patterns of anatomic differences. Structure boundaries from a patient with clinically determined Alzheimer's disease (top left) are overlaid on a cryosection atlas (top right), which has been registered to it using a simple linear transformation. A surface-based image warping algorithm is applied to drive the atlas into the configuration of the patients anatomy ([70]; bottom left). Histologic and neurochemical maps accessible only postmortem can be transferred onto the living subject's scan [22]. The amount of deformation required can be displayed as a tensor map (here only two components of the fully 3D transformation are shown). Tensor maps, and derived vector or scalar fields, can be analyzed in a statistical setting to examine anatomic variation, detect pathology, or track structural changes over time.

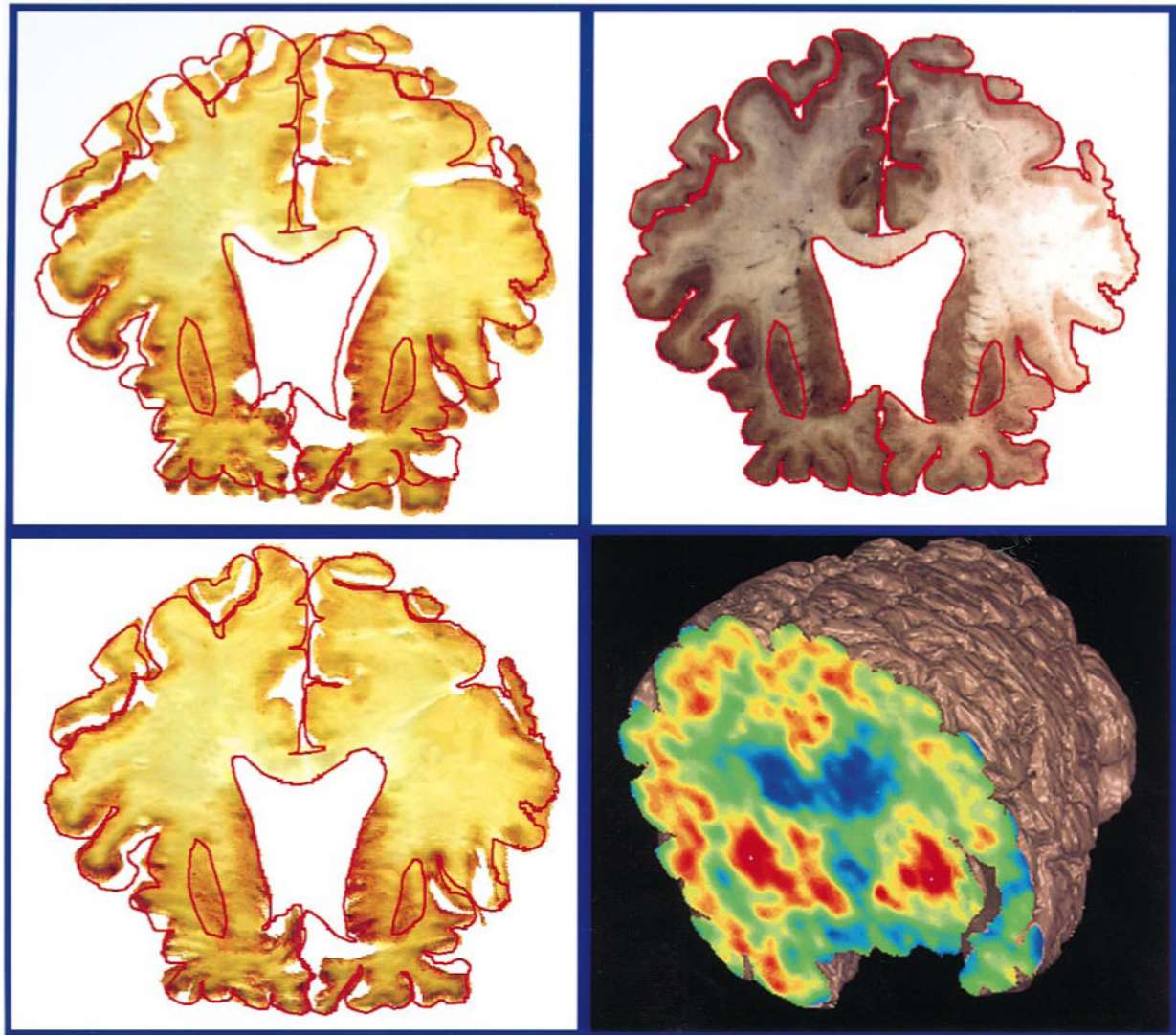
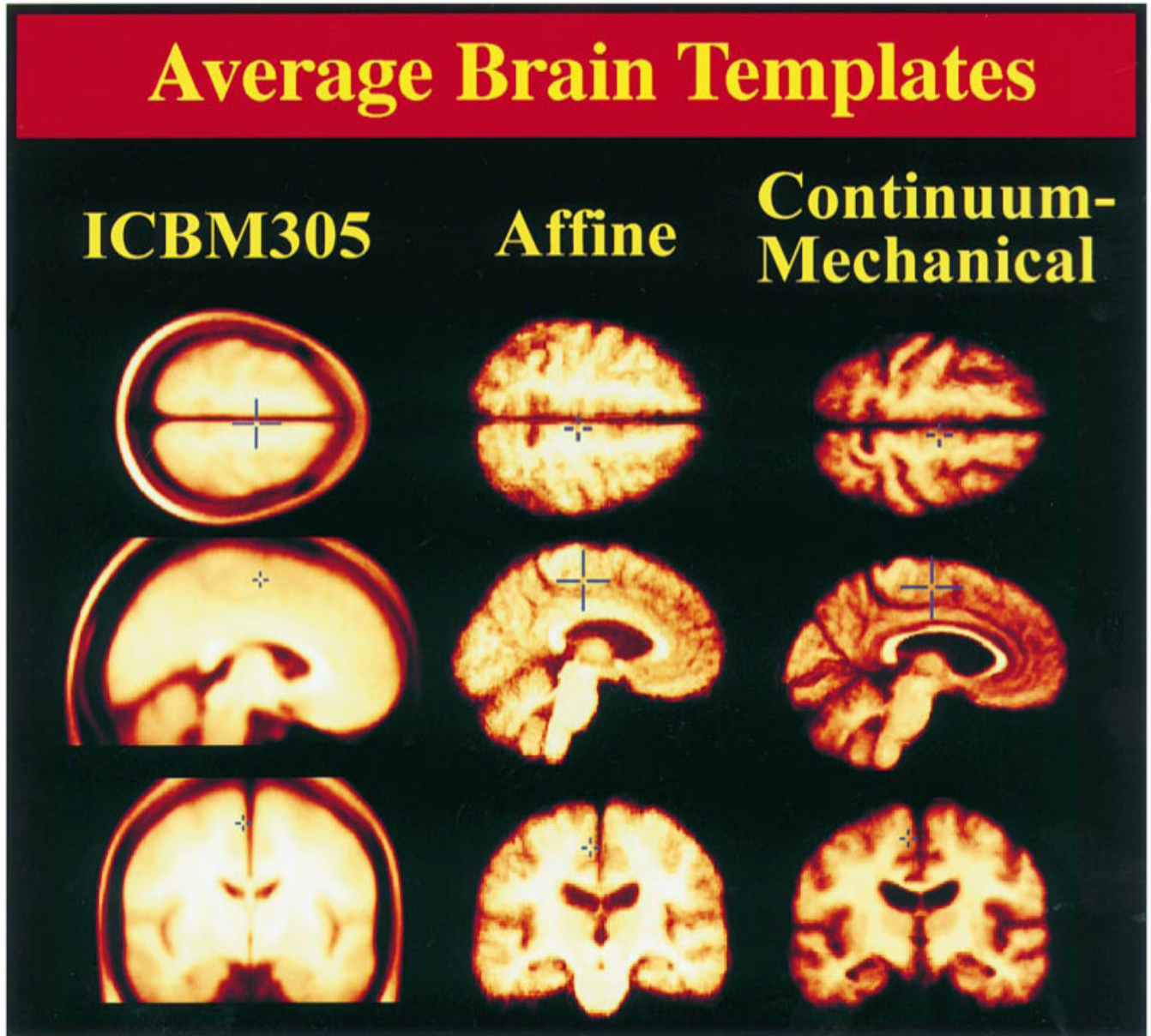


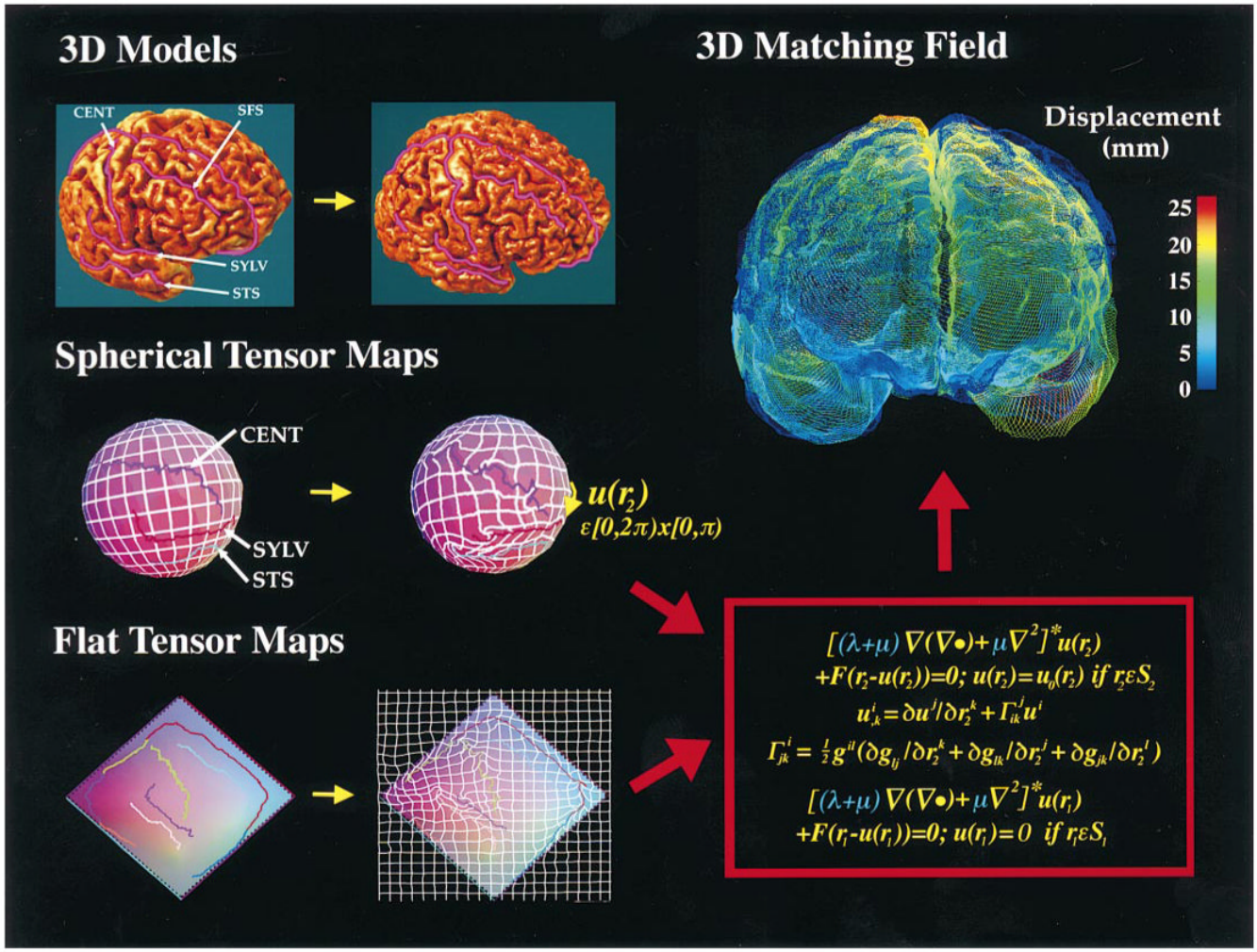
Fig. 5.

Warping algorithms integrate multi-modality brain data. Histologic tissue sections, stained here to reveal neurofibrillary tangle density in a subject with Alzheimer's disease, can be compared with functional imaging data acquired from the same subject *in vivo* [22]. Images of stained tissue sections: (top left) are elastically warped back into their original configuration in the cryosection blockface; (top right) An additional warp reconfigures the post mortem cryosection and histologic data back into their *in vivo* configuration, as imaged by pre-mortem MRI; all maps can then be correlated with PET data acquired *in vivo* from the same patient; (bottom right), which is aligned to the MR template using an additional cross-modality registration. (Data adapted from [22]).

**Fig. 6.**

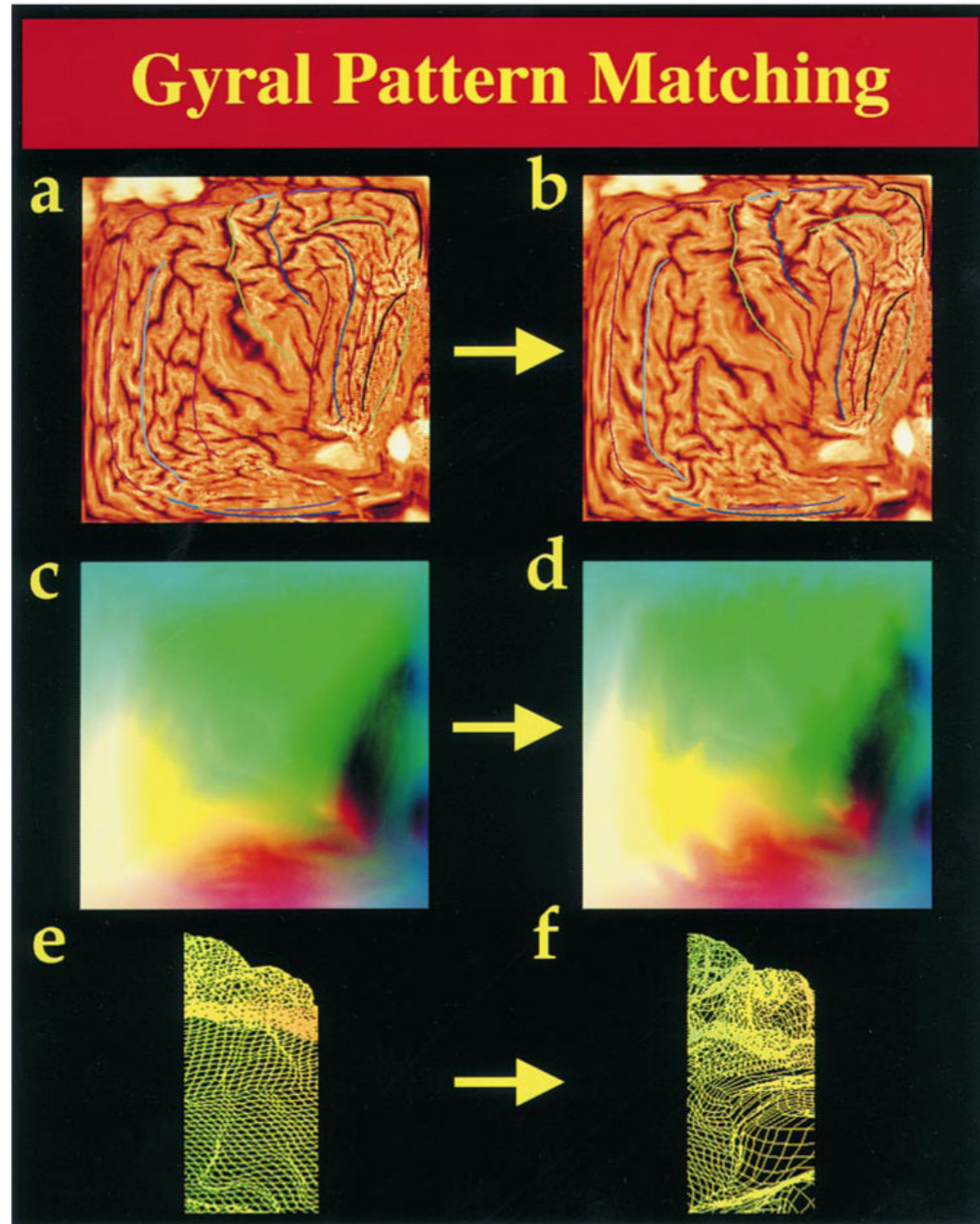
Average brain templates defined using low-order and high-order registration. Axial, sagittal and coronal images are shown from a variety of population-based brain image templates. For comparison purposes: the left column shows a widely used average intensity dataset (ICBM305) based on 305 young normal subjects, created by the International Consortium for Brain Mapping [35]; by contrast, templates in the middle and right columns are average brain templates created from high-resolution 3D MRI scans of Alzheimer's disease patients. (middle column): Affine Brain Template, constructed by averaging normalized MR intensities on a voxel-by-voxel basis after automated affine registration; (right column): Continuum-Mechanical Brain Template, based on intensity averaging after continuum-mechanical transformation. By using spatial transformations of increasing complexity, each patient's anatomy can increasingly be reconfigured into the average anatomical configuration for the group. After intensity correction and normalization, the reconfigured scans are then averaged

on a pixel-by-pixel basis to produce a group image template with the average geometry and average image intensity for the group. Anatomical features are highly resolved, even at the cortex (right column). Transformations of extremely high spatial dimension are required to match cortical features with sufficient accuracy to resolve them after scans are averaged together.

**Fig. 7.**

Maps of the human cerebral cortex: Flat Maps, Spherical Maps, and Tensor Maps. Extreme variations in cortical anatomy (3D Models; top left) present challenges in brain mapping, because of the need to compare and integrate cortically derived brain maps from many subjects. Comparisons of cortical geometry can be based on the warped mapping of one subject's cortex onto another (top right; [93,94]). These warps can also transfer functional maps from one subject to another, or onto a common anatomic template for comparison. Accurate and comprehensive matching of cortical surfaces requires more than the matching of overall cortical geometry. Connected systems of curved sulcal landmarks, distributed over the cortical surface, must also be driven into correspondence with their counterparts in each target brain. Current approaches for deforming one cortex into the shape of another, typically simplify the problem by first representing cortical features on a 2D plane, sphere or ellipsoid, where the matching procedure (i.e. finding $u(r_2)$, above) is subsequently performed [69,70,116,135]. In one approach [93,94], active surface extraction of the cortex provides a continuous inverse mapping from the cortex of each subject to the spherical template used to extract it. Application of these inverse maps to connected networks of curved sulci in each subject transforms the problem into one of computing an angular flow vector field $u(r_2)$, in spherical coordinates, which drives the network elements into register on the sphere (middle panel; [70]). The full mapping (top right) can be recovered in 3D space as a displacement vector field which drives cortical points and regions in one brain into precise structural registration with their

counterparts in the other brain. Tensor Maps (middle and lower left): Although these simple 2-parameter surfaces can serve as proxies for the cortex, different amounts of local dilation and contraction (encoded in the metric tensor if the mapping, $g_{jk}(\mathbf{r})$) are required to transform the cortex into a simpler 2-parameter surface. These variations complicate the direct application of 2D regularization equations for matching their features. A covariant tensor approach is introduced in ([83]; see red box) to address this difficulty. The regularization operator L is replaced by its covariant form L^* , in which correction terms (Christoffel symbols, Γ_{jk}^i) compensate for fluctuations in the metric tensor of the flattening procedure. A covariant tensor approach [83] allows either flat or spherical maps to support cross-subject comparisons and registrations of cortical data by eliminating the confounding effects of metric distortions that necessarily occur during the flattening procedure.

**Fig. 8.**

Gyral pattern matching. Gyral patterns can be matched in a group of subjects to create average cortical surfaces. (a) Shows a cortical flat map for the left hemisphere of one subject, with the average cortical pattern for the group overlaid (colored lines). (b) Shows the result of warping the individual's sulcal pattern into the average configuration for the group, using the covariant field equations (Section 7). The individual cortex (a) is reconfigured (b) to match the average set of cortical curves. The 3D cortical regions that map to these average locations are then recovered in each individual subject, as follows. A color code (c) representing 3D cortical point locations (e) in this subject is convected along with the flow that drives the sulcal pattern into the average configuration for the group (d). Once this is done in all subjects, points on each

individual's cortex are recovered (f) that have the same relative location to the primary folding pattern in all subjects. Averaging of these corresponding points results in a crisp average cortex (Fig. 9). These transformation fields are stored and used to measure regional variability.

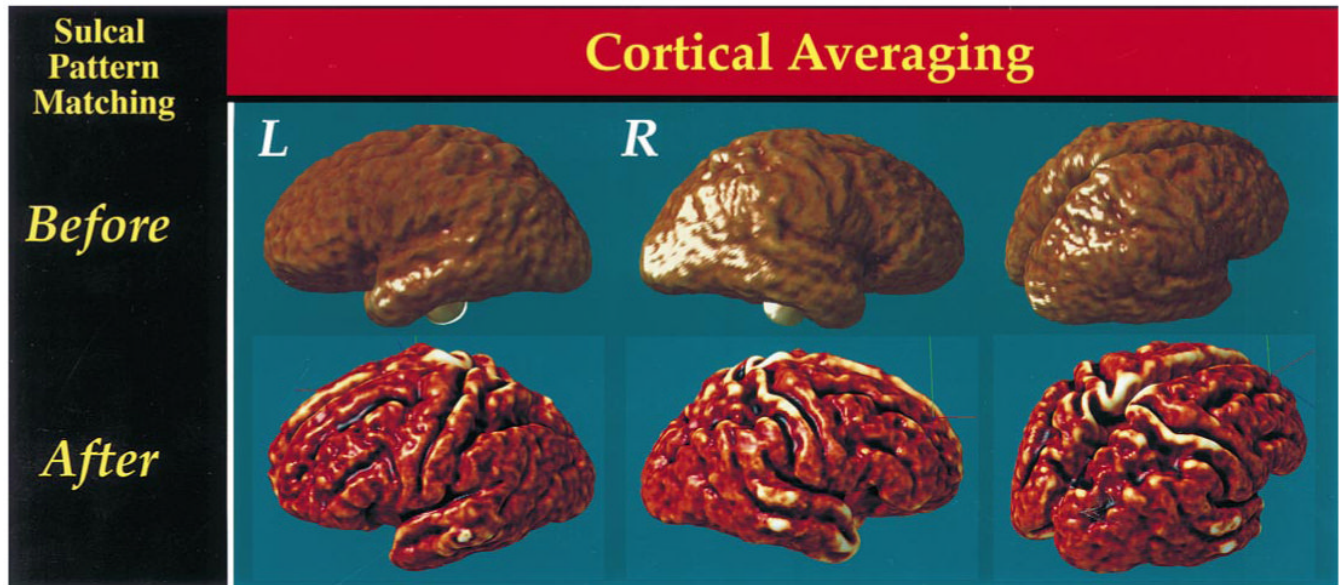
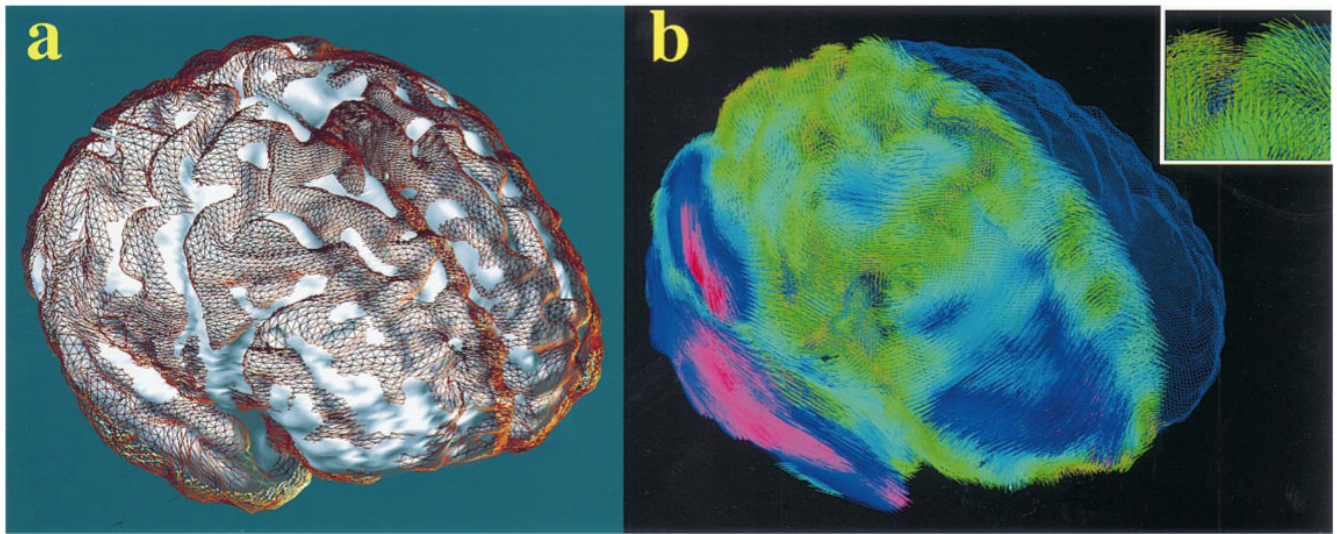


Fig. 9.

Average cortex in Alzheimer's disease. The average cortical surface for a group of subjects ($N=9$, Alzheimer's patients) is shown as a graphically rendered surface model. If sulcal position vectors are averaged without aligning the intervening gyral patterns (top), sulcal features are not reinforced across subjects, and a smooth average cortex is produced. By matching gyral patterns across subjects before averaging, a crisper average cortex is produced (bottom row). Sulcal features that consistently occur across all subjects appear in their average geometric configuration.

**Fig. 10.**

Matching an individual's cortex to the average cortex. 3D variability patterns across the cortex are measured by driving individual cortical patterns into local correspondence with the average cortical model. (a) Shows how the anatomy of one subject (brown surface mesh) deviates from the average cortex (white), after affine alignment of the individual data. (b) Shows the deformation vector field required to reconfigure the gyral pattern of the subject into the exact configuration of the average cortex. The transformation is shown as a flow field that takes the individual's anatomy onto the right hemisphere of the average cortex (blue surface mesh). The largest amount of deformation is required in the temporal and parietal cortex (pink colors, large deformation). Details of the 3D vector deformation field ((b), inset) show the local complexity of the mapping.

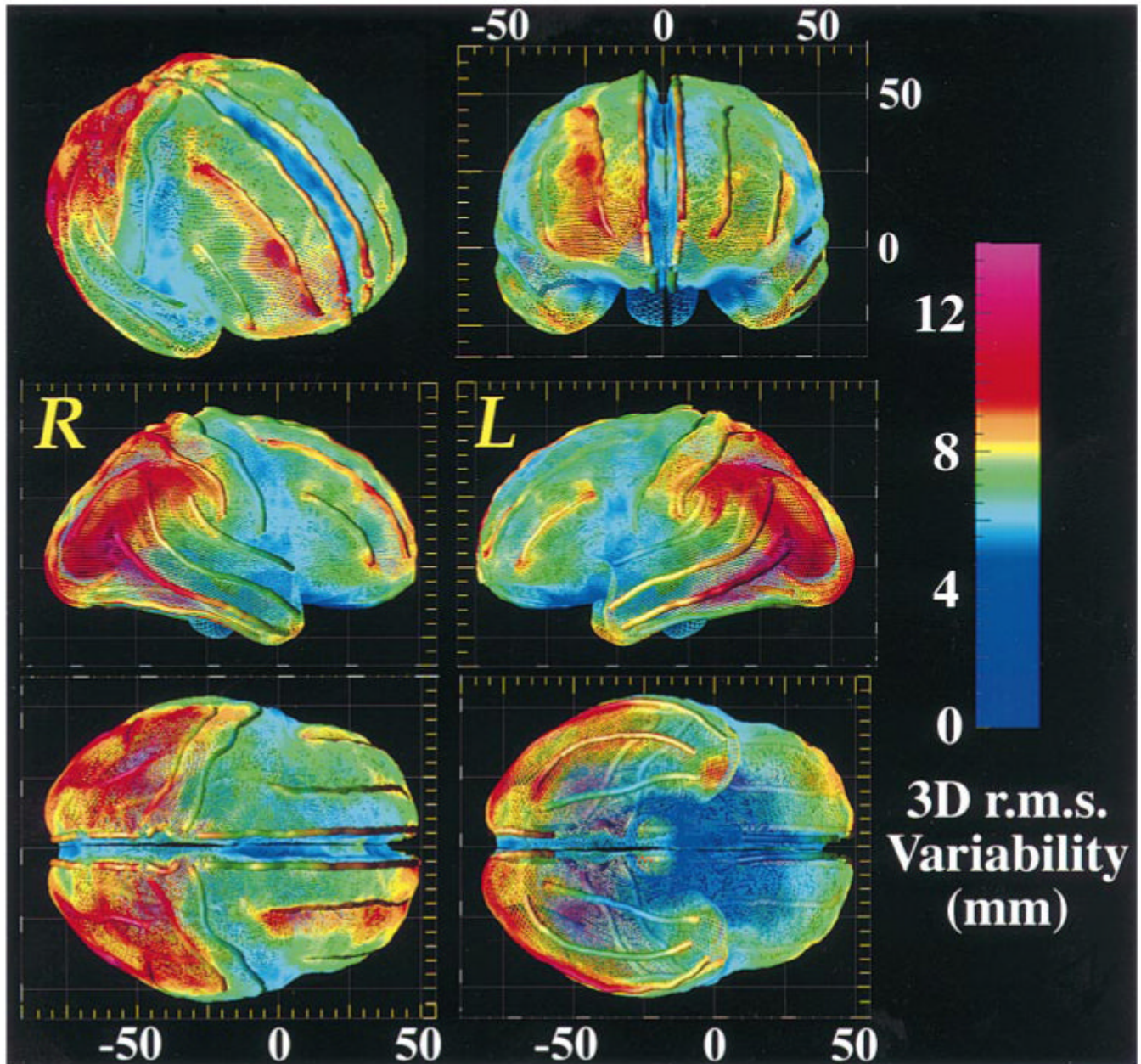
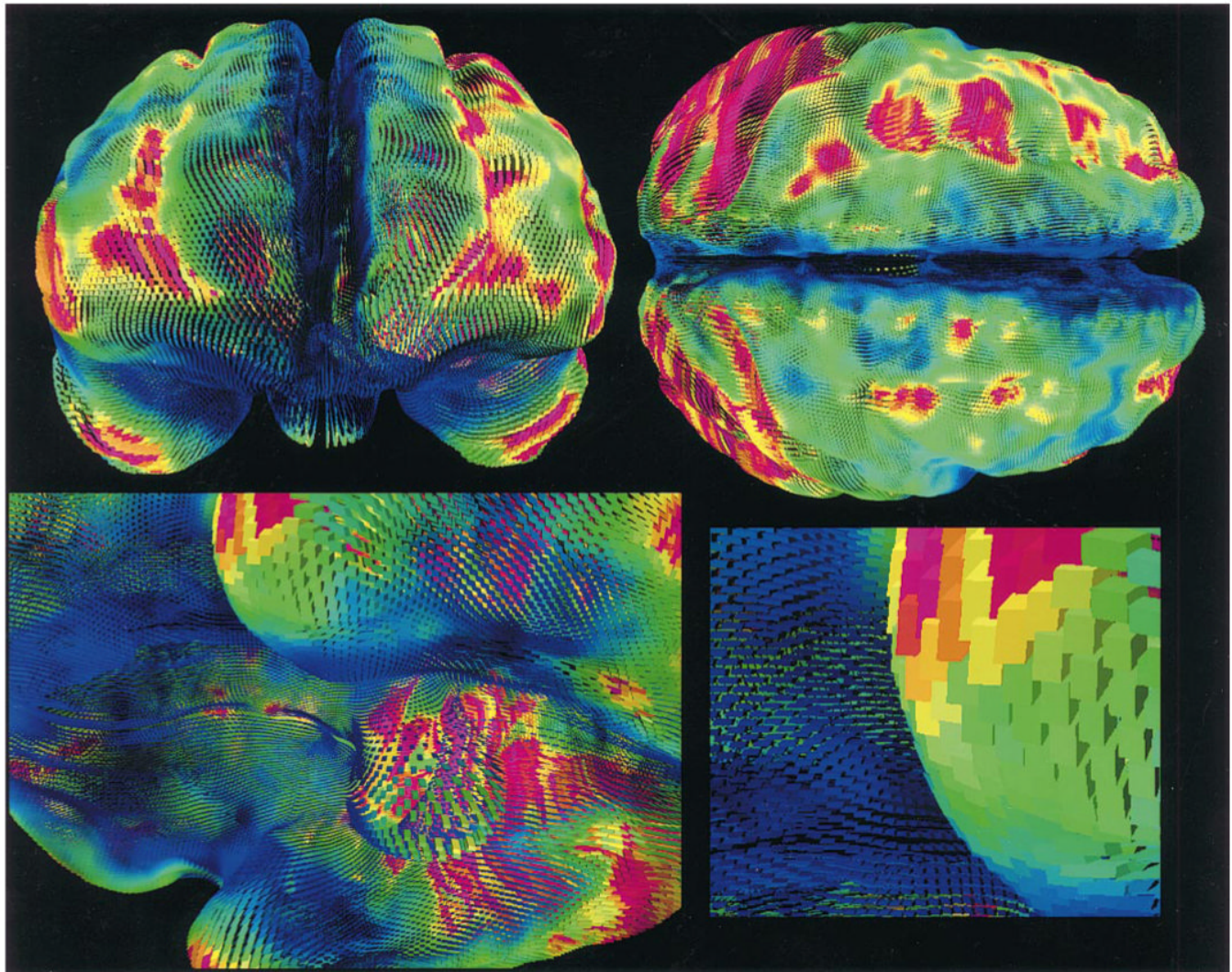


Fig. 11.

3D Cortical variability in Talairach stereotaxic space. (a) The profile of variability across the cortex is shown ($N = 26$ Alzheimer's patients), after differences in brain orientation and size are removed by transforming individual data into Talairach stereotaxic space. The following views are shown: oblique frontal, right, left, top, bottom. Extreme variability in posterior perisylvian zones and superior frontal association cortex (16-18 mm; red colors) contrasts sharply with the comparative invariance of primary sensory, motor, and orbitofrontal cortex (2-5 mm, blue colors).

**Fig. 12.**

Tensor maps reveal directional biases of cortical variation. Tensor maps can be used to visualize the complex patterns of gyral pattern variation at the cortex. The maps are based on a group of 20 elderly normal subjects. Color distinguishes regions of high variability (pink colors) from areas of low variability (blue). Rectangular glyphs indicate the principal directions of variation — they are most elongated along directions where there is greatest anatomic variation across subjects. Each glyph represents the covariance tensor of the vector fields that map individual subjects onto their group average anatomic representation. The resulting information can be leveraged to distinguish normal from abnormal anatomical variants using random field algorithms, and can define statistical distributions for feature labeling at the cortex (cf. [131, 135]).

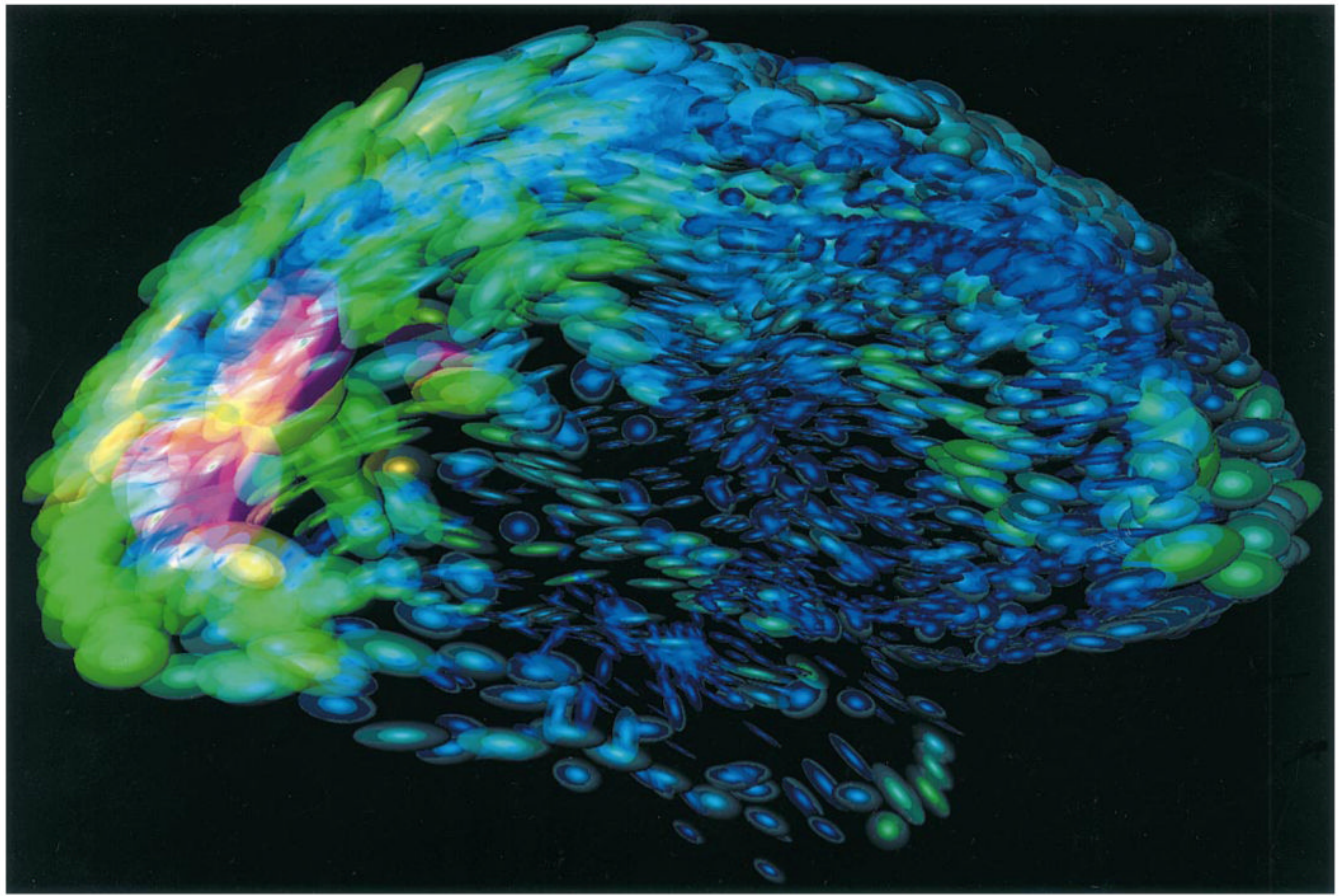


Fig. 13.

Confidence limits on normal anatomic variation: tensor field representation. Again, two tensor maps reveal the preferred directions of cortical variation, after gyral pattern correspondences are taken into account (Figs. 7 and 8). Variability is greatest in temporo-parietal cortex. If cortical variations are modeled as vector field displacements of an average cortical model, ellipsoids of constant probability density can be computed for positions of cortical regions (relative to the average cortex; [54,55]). These ellipsoids are shown, colored by the determinant of the covariance tensor. Fields of ellipsoids ellipses have also been used to visualize multi-directional parameters in diffusion imaging data, and offer a means to represent cortical variability for anomaly detection and Bayesian image labeling.